

# Expression and Function of the Potassium Channels of the Human Heart

PhD Thesis

Balázs Ördög, MSc

Szeged

2009

# Expression and Function of the Potassium Channels of the Human Heart

PhD Thesis

Balázs Ördög, MSc

Supervisors:

Professor János Szabad habil., PhD, DSc  
Professor Zsolt Boldogkői habil., PhD, DSc

Department of Medical Biology  
Faculty of Medicine, University of Szeged

Szeged

2009

## Publications related to the thesis

- I. Ördög B, Brutyó E, Puskás LG, Papp JG, Varró A, Szabad J, Boldogkői Z.  
Gene expression profiling of human cardiac potassium and sodium channels.  
International Journal of Cardiology; 2006; 111: 386–393.  
IF: 2.234
  
- II. Prorok J, Kovács PP, Kristóf AA, Nagy N, Tombácz D, Tóth JS, Ördög B, Jost N, Virág L, Papp JG, Varró A, Tóth A, Boldogkői Z.  
Herpesvirus-mediated delivery of a genetically encoded fluorescent Ca(2+) sensor to canine cardiomyocytes.  
Journal of Biomedicine and Biotechnology; 2009; 2009:361795.  
IF: 2.563
  
- III. Ördög Balázs és Szabad János.  
Miért dobog a szívünk?  
Természet Világa; 2006; 137: 103-108.

Cumulative impact factor: 4.797

## Contents

CONTENTS.....	1
AIM OF THE STUDY.....	2
INTRODUCTION .....	3
<i>Resting potential</i> .....	3
<i>Action potential</i> .....	4
<i>Excitation contraction coupling in the heart</i> .....	6
<i>The heartbeat</i> .....	7
<i>Structure-function relationships of the cardiac ion channels</i> .....	9
<i>Molecular bases of cardiac ion currents</i> .....	12
<i>Channel disorders</i> .....	15
<i>Viral gene transfer into cardiomyocytes</i> .....	17
The Pseudorabies virus .....	18
Lentivirus vectors.....	19
<i>RNA interference</i> .....	22
MATERIALS AND METHODS .....	25
<i>Tissue samples</i> .....	25
<i>Atrial cardiomyocyte and cardiac fibroblast isolation</i> .....	25
<i>Ventricular cardiomyocyte isolation</i> .....	25
<i>Whole-cell patch clamp</i> .....	26
<i>Generation of recombinant PRV strains</i> .....	26
<i>Generation of shRNA<sub>mir</sub> expressing lentivectors</i> .....	27
<i>Gene expression profiling in human cardiac tissue samples</i> .....	28
<i>Validating MiRP2 knock-down in cardiac fibroblasts</i> .....	29
<i>Statistics</i> .....	30
RESULTS.....	30
<i>Expression pattern of K<sup>+</sup>-channel genes in the human heart</i> .....	30
The I <sub>to</sub> -related K <sup>+</sup> channel subunits.....	31
The I <sub>Kur</sub> -related channel subunits .....	31
The I <sub>Kr</sub> - and I <sub>Ks</sub> -related subunits.....	31
Modulatory ‘silent’ subunits of the K <sup>+</sup> channels.....	31
Auxiliary subunits of the voltage gated K <sup>+</sup> channels .....	32
The I <sub>K1</sub> - related inward rectifiers.....	32
The I <sub>K-ATP</sub> channel subunits .....	33
<i>Herpes-virus mediated gene transfer into cardiomyocytes</i> .....	34
<i>Role of the MiRP2 regulatory subunit in I<sub>to</sub> channels</i> .....	35
Validating MiRP2 mRNA knock-down in canine atrial fibroblasts .....	35
Effect of MiRP2 knock-down on macroscopic I <sub>to</sub> parameters .....	36
Current-voltage relations .....	38
Voltage-dependence of activation and inactivation .....	38
Time course of activation and inactivation.....	39
DISCUSSION.....	40
<i>Expression pattern of K<sup>+</sup>-channel genes in the human heart</i> .....	40
The I <sub>to</sub> -related K <sup>+</sup> channel subunits.....	41
The I <sub>Kur</sub> -related channel subunits .....	42
Modulatory ‘silent’ alpha-subunits of K <sup>+</sup> channels.....	42
Auxiliary subunits of the K <sup>+</sup> channels.....	43
<i>Herpes-virus mediated gene transfer into cardiomyocytes</i> .....	43
<i>Role of MiRP2 regulatory subunit in I<sub>to</sub> channels</i> .....	44
SUMMARY .....	46
REFERENCES .....	47
ACKNOWLEDGEMENTS .....	52

## Aim of the study

The spatial and temporal regulation of muscle contraction in the heart is based on region-specific action potential configurations. The action potential, which is the change of membrane potential in time, is the result of the subtly balanced and concerted action of the underlying ion currents driven by transmembrane ion channels. Under pathophysiological conditions, changes in ion currents result in abnormal action potential waveforms which may provide an arrhythmogenic substrate and lead to life threatening arrhythmias or sudden cardiac death. Ion channels - the main objectives of our study - are protein complexes formed by pore-forming and regulatory ion channel subunits. The pore-forming subunits serve as pathways for ions through the cell membrane, while the regulatory subunits are substantial modifiers of ion channel function. The ion channel function depends primarily on the subunit composition of the ion channel complex. The ion currents have been thoroughly characterized by electrophysiological and pharmacological methods, however, little is known about the subunit composition of the ion channel complexes. Revealing the subunit composition of the ion channels and determining the subunit-specific function of individual ion channel subunits would help us not only to understand better how the heart is functioning both under normal and pathophysiological conditions, but with the gene therapy on the horizon, it would also open avenues for novel therapeutic approaches. The aim of the present study is the development of an experimental system to characterize the specific function of individual ion channel subunits in heart muscle cells *ex vivo* and potentially *in vivo*. The first project described here was designed to quantitatively measure the expression level of a comprehensive set of ion channel subunit-coding genes, with particular emphasis on potassium channel genes, in two regions of the normal human heart by the real time PCR technique. Based on the gene expression data we aim to conclude which ion channel subunits are expressed in the human myocardium and which of them could have physiological importance. In the second project we explore possibilities to utilize *Pseudorabies virus* as a general vehicle for delivering genetic material into heart muscle cells *ex vivo*. In our third project we apply lentivirus delivered artificial microRNAs to study the function of potassium channel subunits in cardiomyocytes. We particularly focus on MiRP2, a novel member of the KCNE gene family, of which a possible function has been proposed based on *in vitro* data, but has not been confirmed *ex vivo* or *in vivo*. We show direct evidence for the regulatory role of MiRP2 in the transient outward potassium channels in cardiomyocytes.

## Introduction

### Resting potential

Every living cell is surrounded by the cell membrane. The cell membrane is composed of a lipid bilayer and various protein molecules. The lipid bilayer is not permeable for charged and large molecules and is thus an excellent insulator. Some of the protein molecules embedded in the cell membrane form pores across the lipid bilayer. The two most important types of pore-forming membrane proteins are the ion channels and the ion pumps. Ion channels facilitate the passive diffusion of ions across the cell membrane. Ions move through ion channels according to their concentration and electric gradients without energy consumption. Most types of the ion channels possess selectivity for certain types of ions and thus there are potassium-, chloride- and sodium-selective ion channels. Ion pumps, by using ATP stored energy, transport ions against their electrochemical gradients.

In cardiomyocytes, the cytoplasmic surface of the membrane is more negative than the outer membrane surface and hence a transmembrane potential can be recorded. In resting cardiomyocytes the membrane potential ranges from -50 to -95mV, depending on the cardiac cell type. The basis of membrane potential is the differential distribution of several inorganic ions, mostly  $K^+$ ,  $Na^+$ ,  $Ca^{2+}$ ,  $Cl^-$  and proteins carrying negative charge, on the two sides of the cell membrane (Figure 1). The cell membrane is impermeable for protein anions, of which concentration is constantly higher in the intracellular space than outside the cell. The differential distribution of inorganic ions is generated and maintained by the ion pumps. The most important ion pump is the  $Na^+/K^+$  pump.

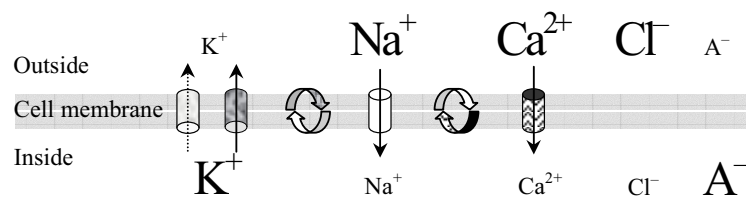


**Figure 1.** Differential distribution of cations and anions on two sides of the cell membrane. The figure indicates the most important ion channel types and ion pumps that are involved in the generation and maintenance of the resting potential.  $A^-$  represents negatively charged proteins. The size of the letters refers to the different ion concentrations. The dotted arrow shows  $K^+$  movement through the non-voltage-gated channels, solid arrows indicate the voltage-gated channel types. The direction of arrows corresponds to the direction of ion movement through open channels. The  $\odot$  symbols stand for  $Na^+/K^+$  and a  $Na^+/Ca^{2+}$  ion pumps.

The  $\text{Na}^+/\text{K}^+$  pump transports three  $\text{K}^+$  ions from the extracellular space to the cytoplasm and two  $\text{Na}^+$  ions at the same time in the opposite direction. Due to the never-ending activity of the  $\text{Na}^+/\text{K}^+$  pump the cytoplasm is poor in  $\text{Na}^+$  and rich in  $\text{K}^+$ , while the extracellular space is rich in  $\text{Na}^+$  and poor in  $\text{K}^+$  (Figure 1).

The resting membrane potential can be modeled by the Nernst and the Goldman-Hodgkin-Katz (GHK) equations (Figure 2 and 3). The Nernst equation gives the equilibrium potential for a given ion, a potential at which the ionic flux is zero. The equilibrium potential for a given ion depends solely on its concentration on the two sides of the membrane and on temperature (Figure 2). The membrane of resting cardiomyocytes is permeable mostly for  $\text{K}^+$  only, while membrane permeability for other ions is relatively low. Therefore the resting membrane potential is very close to the equilibrium potential of  $\text{K}^+$ . When concentrations and relative permeabilities of other ions are taken into account, the membrane potential is calculated by the GHK equation (Figure 3).

$$E_{eq, K^+} = \frac{RT}{zF} \ln \frac{[K^+]_o}{[K^+]_i}$$

**Figure 2.** The Nernst equation.  $E_{eq, K^+}$  is the equilibrium potential for  $\text{K}^+$  ion in Volts,  $R$  is the universal gas constant,  $T$  is the absolute temperature,  $z$  is the number of elementary charges of the ion in question and  $F$  is the Faraday constant,  $[K^+]_o$  is the extracellular concentration of  $\text{K}^+$  and  $[K^+]_i$  is the  $\text{K}^+$  concentration in the cytoplasm.

$$E_m = \frac{RT}{F} \ln \left( \frac{P_{Na^+} [Na^+]_o + P_{K^+} [K^+]_o + P_{Cl^-} [Cl^-]_i}{P_{Na^+} [Na^+]_i + P_{K^+} [K^+]_i + P_{Cl^-} [Cl^-]_o} \right)$$

**Figure 3.** The Goldman-Hodgkin-Katz equation.  $E_m$  is the membrane potential,  $R$ ,  $T$  and  $F$  are as in Figure 2,  $P_X$  is membrane permeability for ion  $X$  and  $[X]_i$  and  $[X]_o$  are the cytoplasmic and extracellular concentrations of  $X$  ion, respectively.

### Action potential

Excitable cells like heart muscle cells respond to proper stimulus by characteristic changes in membrane potential. This change in the membrane potential is termed action potential.

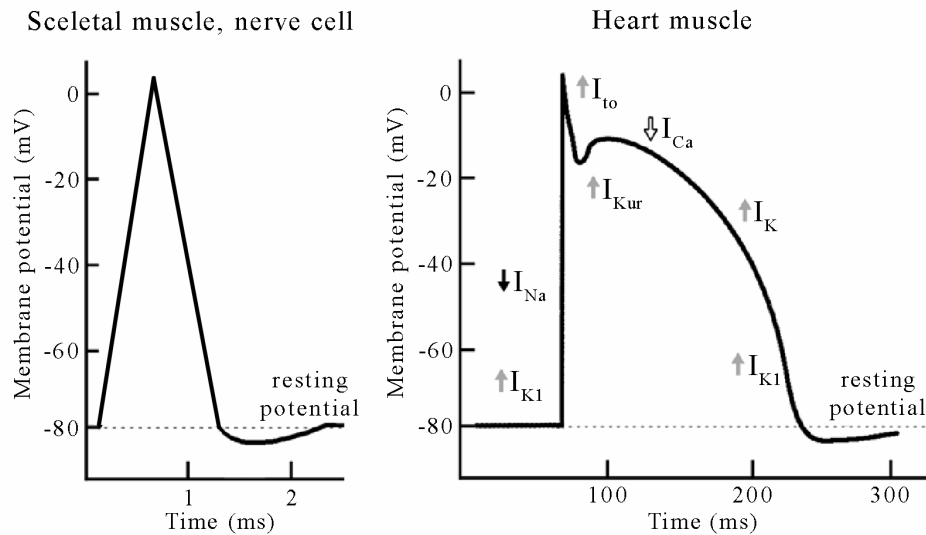


**Figure 4.** Action potential in nerve, skeletal and heart muscle cells. Note the different time scales of the two diagrams. Cardiac action potential is the result of the concerted action of the various ion channel types. While the  $K^+$  channels lead to outward ( $\uparrow$ ) currents ( $I_{K1}$ ,  $I_{to}$ ,  $I_{Kur}$  and  $I_K$ ), the  $Na^+$  and the  $Ca^{2+}$  channels facilitate inward ( $\downarrow$ ) flow of  $Na^+$  and  $Ca^{2+}$  ions, respectively ( $I_{Na}$  and  $I_{Ca}$ ).

The basis of the action potential is a sequential change in membrane permeability for certain types of ions. During cardiac action potential the membrane permeability changes due to the activity of voltage-gated ion channels. The voltage-gated  $Na^+$  and the  $Ca^{2+}$  selective channels drive inward  $Na^+$  and  $Ca^{2+}$  currents, while the  $K^+$  selective channels drive outward  $K^+$  currents.

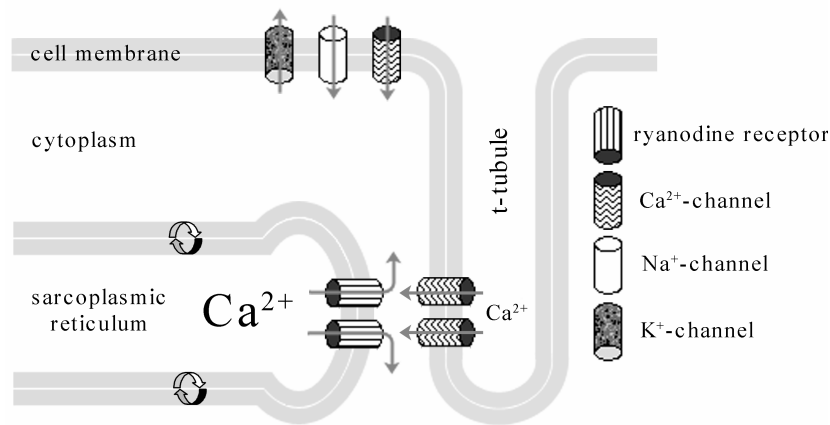
In the cardiac action potential 5 phases are generally distinguished (Figure 4) (70). Phase zero is the rapid depolarization or ‘upstroke’ of the membrane potential. In phase zero  $Na^+$  channels open ( $I_{Na}$ , Figure 4) in response to a depolarizing stimulus large enough to reach a threshold. The  $Na^+$  influx lasts only a few milliseconds and as the intracellular  $Na^+$  concentration increases, the driving force for the  $Na^+$  decreases. There is no more  $Na^+$  influx when the membrane potential reaches the equilibrium potential for  $Na^+$  and the  $Na^+$  channels are functionally inactivated. In phase one the membrane potential rapidly and transiently returns near to 0 mV partly due to the inactivation of the  $Na^+$  channels and to the opening of the so-called transient outward  $K^+$  channels ( $I_{to}$ , Figure 4). The magnitude of the transient outward  $K^+$  current determines the height and duration of the forthcoming phase of the action potential, the so-called plateau phase (phase two). During the plateau phase there is a dynamic

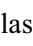


balance between  $\text{Ca}^{2+}$  influx ( $I_{\text{Ca}}$ , Figure 4) driven by voltage-gated  $\text{Ca}^{2+}$  channels and  $\text{K}^{+}$  efflux, hence the membrane potential is almost stable or only slightly decreases. In phase three the  $\text{Ca}^{2+}$  influx decreases because of the inactivation of the  $\text{Ca}^{2+}$  channels while an outward current increases mainly because of the activation of the so-called delayed rectifier  $\text{K}^{+}$  channels ( $I_{\text{K}}$ , Figure 4) and the membrane potential returns to more negative ranges. In phase four beside  $I_{\text{K}}$  the so-called inward rectifier  $\text{K}^{+}$  channels are involved ( $I_{\text{K1}}$ , Figure 4). The differential distribution of ions that are typical for the resting membrane are rearranged mainly by the action of the  $\text{Na}^{+}/\text{K}^{+}$  pump and the  $\text{Na}^{+}/\text{Ca}^{+}$  exchanger. The  $\text{Na}^{+}/\text{Ca}^{+}$  exchanger is an antiporter that facilitates the transport of  $\text{Ca}^{2+}$  ions out from the cytoplasm with the help of the  $\text{Na}^{+}$  concentration gradient.

### **Excitation contraction coupling in the heart**

The direct trigger for muscle contraction is the release of  $\text{Ca}^{2+}$  from the sarcoplasmic reticulum (SR) (21). The  $\text{Ca}^{2+}$  release is induced by  $\text{Ca}^{2+}$  ions and is manifested by the voltage-gated  $\text{Ca}^{2+}$  channels during phase 1 and phase 2 of the action potential. The phenomenon is called the  $\text{Ca}^{2+}$  induced  $\text{Ca}^{2+}$  release. The heart muscle cells, like the striated muscle cells are enmeshed by invaginations of the sarcolemma (Figure 5). These invaginations are the transversal tubules (t-tubules). At certain places the membrane of the t-tubules and the membrane of the SR are very close to each other. They are so close that the voltage-gated  $\text{Ca}^{2+}$  channels of the cell membrane and the  $\text{Ca}^{2+}$  channels of the SR, the so-called ryanodine receptors are placed in direct vicinity of each other. The ryanodine receptor is basically a  $\text{Ca}^{2+}$  sensitive  $\text{Ca}^{2+}$  channel. It opens whenever the cytoplasmic  $\text{Ca}^{2+}$  concentration is elevated. Thus in the phase one and two of the action potential the  $\text{Ca}^{2+}$  ions that flow through the voltage-gated  $\text{Ca}^{2+}$  channels of the sarcolemma and arrive to the cytoplasmic surface of the ryanodine receptors induce opening of the ryanodine receptor. The  $\text{Ca}^{2+}$  needed for muscle contraction is then released from the  $\text{Ca}^{2+}$  store through the open ryanodine receptors. When the task of the cardiomyocytes is completed and their microfilaments should be released the  $\text{Ca}^{2+}$  ions are removed from the cytoplasm mostly by the  $\text{Ca}^{2+}$  pumps built into the membrane of the SR (Figure 5). However, in most mammalian ventricular myocytes the SR  $\text{Ca}^{2+}$  pumps account for about 60-70% of the  $\text{Ca}^{2+}$  uptake and the rest 30-40% is removed by the sarcolemmal  $\text{Na}^{+}/\text{Ca}^{2+}$  exchanger molecules and by the sarcolemmal  $\text{Ca}^{2+}$  pumps.



**Figure 5.** Distribution of ion channels in the sarcolemma, in the t-tubule membrane and in the membrane of the sarcoplasmic reticulum. The  symbols stand for Ca<sup>2+</sup> pumps of the sarcoplasmic reticulum.

In both the skeletal and in heart muscles, the action potentials regulate the duration and strength of muscle contraction. In the skeletal muscles the duration of the action potential is shorter than the duration of the shortening of muscle filaments. Thus additional action potentials may take place while muscle filaments are still shortened and a continuous contraction can be maintained. In the heart, a continuous contraction would completely abolish pump function and it never happens under normal conditions. Cardiac action potential takes longer time than contraction does, so heart muscle filaments relax before the action potential is completed. A new action potential can be initialized only when the myofilaments are relaxing, which thus ensures the rhythmical function of the heart.

### The heartbeat

The proper pump function of the heart depends on regular generation of action potentials and the well-organized conduction of the stimulus through electrically coupled cells by gap junctions or through the specific excitation conduction system of the heart (Figure 6). While contraction of the skeletal muscles is induced by action potentials generated in the nervous system, the heart does not need external stimulus for contraction and beating. There is a specialized portion of the heart positioned in the wall of the right atrium, called the sinoatrial node (SAN) that controls heart beats (Figure 6). The modified heart muscle cells of the SAN perform only weak contractions. However they possess the ability to generate action potentials and regulate contractions in the entire heart. This function of the SAN is known of pacemaker activity. Hence there is no stimulus conduction system in the atria, action potential

generated in the SAN spreads through the muscle cells of the left and right atrium and induces contraction. The atria and the ventricles are electrically insulated by a fibrous connective tissue. The so-called atrio-ventricular node (AVN), placed between the atria and ventricles, is the only path through which action potentials can reach the ventricles.

The SAN is the primary pacemaker of the heart, however, in the absence of SAN function, or when conduction is blocked, cells of the AVN, or cells in the Purkinje fiber are also able to generate action potentials. However, without the primary pacemaker function the heart rate drastically slows down. The action potential suffers a few milliseconds delay after reaching the AVN and before traveling further towards the ventricles. The short delay allows the blood to be pumped out from the atria while the ventricles are still in diastole. For an effective pump function muscle cells of both ventricles have to be excited at almost the same time. For this purpose the action potential is driven from the AVN through the specific excitation conduction system of the heart. The excitation conduction system is composed of the His bundles, the Tawara branches and the Purkinje fibers and contains modified heart muscle cells that were “designed” to conduct excitation (Figure 6). The His bundles and the Tawara branches are placed in the septum while Purkinje fibers enmesh the walls of both ventricles. The His bundles and the Tawara branches lead action potential effectively from the AVN to the network of Purkinje fibers where the excitation spreads toward the muscle cells of the wall of the ventricles and triggers contraction.

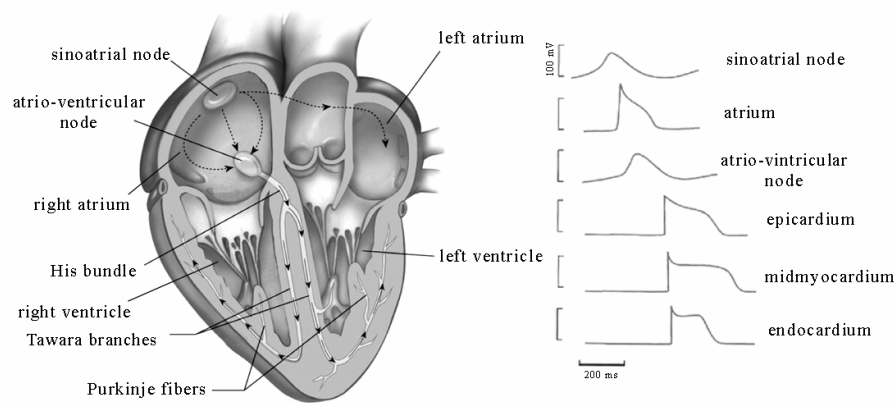


**Figure 6.** The pacemaker and the excitation conduction system of the heart. Schematic diagrams of specific action potential waveforms in the different regions of the heart are shown on the right panel.

### Structure-function relationships of the cardiac ion channels

The central role of ions in the excitability of nerve and muscle has been first described by Sidney Ringer and Walther Nernst in the 1880s. A decade later Julius Bernstein correctly proposed that excitable cells are surrounded by a membrane selectively permeable to certain ions. However, experimental evidences for the existence of ion channels appeared only in the early 1980s when Erwin Neher and Bert Sakmann developed the patch-clamp technique (62). Analysis of ion channels at the molecular scale began in 1984 when the  $\text{Na}^+$  channel gene of the electric eel was cloned (46). The molecular techniques made the analysis of the biophysical properties of ion currents and ion channels possible. The most prominent step in understanding the structure of ion channels was achieved by Roderick MacKinnon and his colleagues who determined the structure of the bacterial *KcsA*  $\text{K}^+$  channel (18). It appears that despite the enormous functional heterogeneity of the different ion channel types they are built up from the same or similar structural units. Therefore, findings achieved from the studies made on the bacterial *KcsA* channel may be applied to most of the ion channels of higher animals including humans.

Every known ion channel is composed of two basic structural elements, the transmembrane  $\alpha$ -helices and the so-called pore domain (Figure 7). While transmembrane helices mostly serve as a 'scaffold' of the ion channel, the pore domain determines the shape of the pore in the ion channel and contribute to basic properties of the channel like selectivity and conductivity. The most simple ion channels are the inwardly rectifying  $\text{K}^+$  channels (31) that resemble to the bacterial *KcsA* channel (Figure 7). One functional inwardly rectifying  $\text{K}^+$  channel is composed of four subunits. The subunits are structurally identical, even though they may be products of different genes. One subunit of an inwardly rectifying  $\text{K}^+$  channel consists of two transmembrane  $\alpha$ -helices and one pore domain between the two helices. The cardiac voltage-gated  $\text{K}^+$  channels are also tetramers (64). One subunit of a voltage-gated  $\text{K}^+$  channel consists of six transmembrane helices and one pore domain between the two most C-terminal helices. The cardiac  $\text{Na}^+$  and  $\text{Ca}^{2+}$  channels are composed of a single polypeptide chain, however, these huge proteins consist of four domains. One of their domains corresponds to one subunit of the voltage-gated  $\text{K}^+$  channels (Figure 7). The last class of the cardiac ion channels discovered is the so-called two pore domain  $\text{K}^+$  channels (Figure 7). The two pore domain channels are dimers composed of two structurally identical subunits (36).

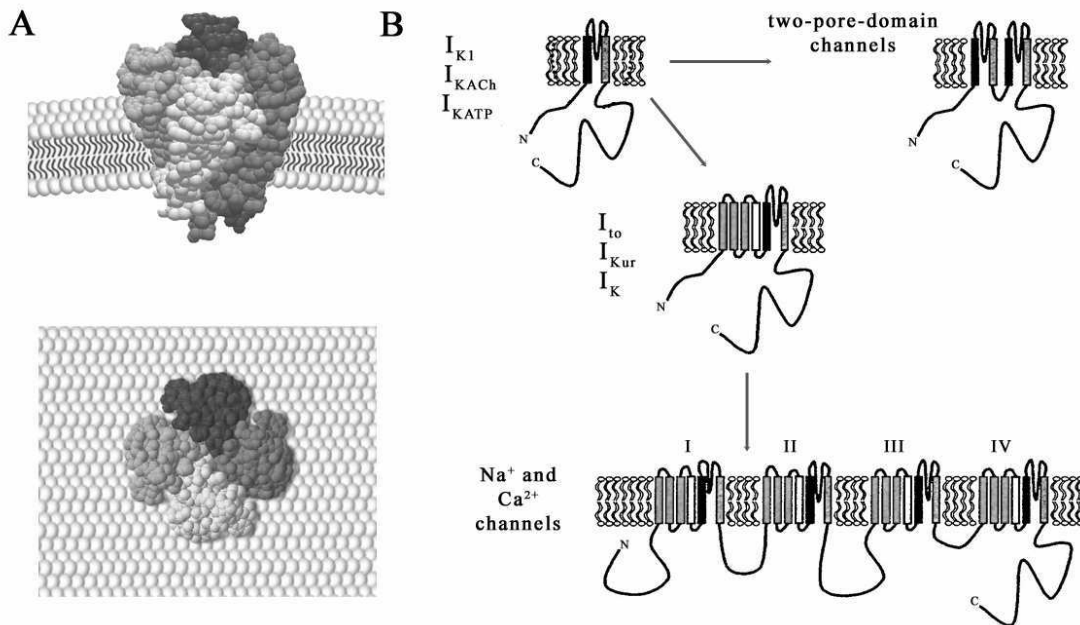


**Figure 7.** Three dimensional structure of the bacterial KcsA channel (A). Tertiary structure of different cardiac ion channel types (B).

One subunit contains two domains and the structure of each domain is identical with the structure of an inwardly rectifying  $K^+$  channel-forming subunit. There is a schematic illustration of the structure of an inwardly rectifying  $K^+$  channel in Figure 8. It is the narrow bottleneck-shaped portion of the pore of the channel that is probably the most important with respect to channel function. The narrow bottleneck-shaped portion of the pore is often called the selectivity filter of the channel, hence the ion selectivity of the channel depends on the dimensions of the bottleneck. The selectivity filter is composed of amino acids of the four pore domains belonging to the four subunits that form the channel. It is 1.2 nm long and 0.28 nm in diameter. Clearly, it is too narrow for a hydrated  $K^+$  ion. Removing the primary hydration shell of the  $K^+$  ion would cost lots of energy. However, ion channels do not consume energy for ion transport. How are the  $K^+$  ions able to pass through the ion channels without using energy? The answer becomes clear when one looks at the high-resolution structure of a  $K^+$  channel. The inner surface of the selectivity filter is covered by carbonyl oxygen atoms that carry partial negative charges and are positioned exactly at the same distance as the distance in between the water molecules in the primary hydration shell of the  $K^+$  ion. Hence,  $K^+$  ions moving through the selective filter can easily interact with the carbonyl oxygen atoms instead of the water molecules. The carbonyl oxygen atoms provide a preferred environment for the  $K^+$  ions and thus the  $K^+$  ions can flow through the channel without using energy. It has been shown that two  $K^+$  ions bind into the selectivity filter at the

same time. Binding of a third  $K^+$  ion is associated with a concerted  $K^+$  ion exit at the other side of the pore giving rise thus to efficient  $K^+$  ion conductance. Other types of ions that differ in size from the  $K^+$  ions can not interact with these oxygen atoms and can not get across the channel.

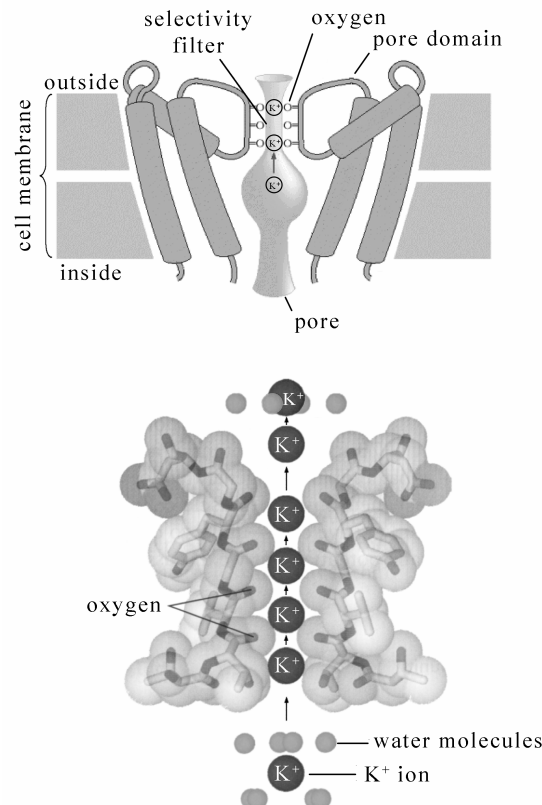


**Figure 8.** Upper panel: schematic illustration of the cross section of the bacterial KcsA channel. Lower panel: ion selectivity depends on dimensions of the selectivity filter.

Effective ion conductance is the basic function that an ion channel accomplishes. However, in case of voltage-gated channels – like cardiac  $Na^+$ ,  $Ca^{2+}$ , transient outward and delayed rectifying  $K^+$  channels – another important task is needed to be done. The latter types of channels are voltage-gated implying that they change their behavior depending on the actual value of the membrane potential. In general, cardiac voltage-gated ion channels open with depolarization, are inactivated in the depolarized membrane and they have to recover from this inactivated state before they are able to open again. It has been hypothesized, following the cloning the first  $Na^+$  channel gene, that the fourth transmembrane helix of each subunit of the voltage-gated  $K^+$  channels or the corresponding transmembrane segments of the  $Na^+$  and  $Ca^{2+}$  channels serve as the voltage sensor of the channel (Figure 7 and 9). There are positively

charged amino acids (arginine or lysine) in the voltage sensor transmembrane helices in every 3<sup>rd</sup> position. This set of charged amino acids is present in the fourth transmembrane helices of every known voltage-gated ion channels. The above assumption is further supported by the following observation. When the charged amino acids of the putative voltage sensor were changed to cysteines the opening or closing of the channel was drastically altered (23, 81). It is very likely that the voltage sensor helix moves toward the inner or the outer surface of the membrane depending on the actual membrane potential (Figure 9). Movement of the voltage sensor may induce conformation changes in the entire channel complex resulting in changes in the channel conductance. However, the exact nature of the voltage-dependent conformation rearrangements has not yet been revealed.

Many voltage-gated ion channels like the Na<sup>+</sup>, the Ca<sup>2+</sup> and the transient outward K<sup>+</sup> channels display inactivation, that is, an entry into a non-conducting state during depolarization. Two major mechanisms of inactivation are proposed, namely N- and C-type inactivation (Figure 9). In the N-type inactivation the N-terminus of the channel subunit binds to the cytoplasmic entry site of the pore physically occluding the channel (3). In the C-type inactivation, despite what the terminology suggests, rearrangement of amino acid side chains in or near the pore are involved, similarly to the closing of the shutter on a camera (29).

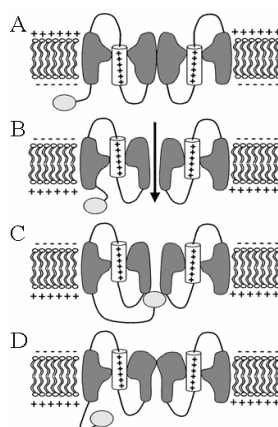


**Figure 9.** Conformation transitions in voltage-gated ion channels. **A:** resting state; **B:** open state in the depolarized membrane; **C:** N-type inactivation; **D:** C-type inactivation.

### Molecular bases of cardiac ion currents

Revealing molecular features of the cardiac ionic currents is like building a bridge between electrophysiology and molecular biology. The majority of the conclusions are drawn in the light of expression levels of the ion channel subunit coding genes in the heart muscle and

through comparing the electrophysiological properties of the currents produced by cloned and heterologously expressed ion channel subunits to native cardiac currents. Isolating mutations in ion channels genes with known effect in ion channel related diseases may also provide useful information.

Interestingly, in case of the inward currents the molecular bases of the ionic currents are well founded. The voltage gated  $\text{Na}^+$  channel gene family counts 11 members named as *SCN1A* to *SCN11A*. Each member shows similar structure with four six transmembrane helix-containing domains (Figure 7). Most of the gene family members are expressed in the central nervous system, while in the heart only the fifth isoform is present (4) (*SCN5A*, Table 1). It is the cardiac variant of voltage gated  $\text{Na}^+$  channels that is responsible for the depolarization events in most of the cardiac tissue types.

**Table 1.** Molecular features of cardiac ion currents

Current	Pore forming subunit genes		Auxiliary subunit genes	
	Kv name	KCN name	Kv name	KCN name
$I_{\text{NA}}$	$\text{Na}_v1.5$	<i>SCN5A</i>	$\beta 1$ $\beta 2$	<i>SCN1B</i> <i>SCN2B</i>
$I_{\text{Ca}}$ T-type	$\text{Ca}_v3.2$	<i>CACNA1H</i>	$\beta 1$ $\beta 2$ $\alpha 2\delta$	<i>CACNAB1</i>
L-type	$\text{Ca}_v1.2$	<i>CACNA1C</i>		<i>CACNAB2</i>
				<i>CACNA2D1</i>
$I_{\text{to}}$	$\text{Kv}1.4$	<i>KCNA4</i>	KChIP2	<i>KCNIP2</i>
	$\text{Kv}4.3$	<i>KCND3</i>		
$I_{\text{Kur}}$	$\text{Kv}1.5$	<i>KCNA5</i>	$\text{Kv}\beta 1$	<i>KCNAB1</i>
			$\text{Kv}\beta 2$	<i>KCNAB2</i>
$I_{\text{K}}$ (slow)	$\text{KvLQT1}$	<i>KCNQ1</i>	Mink	<i>KCNE1</i>
$I_{\text{K}}$ (rapid)	HERG	<i>KCNH2</i>	Mink	<i>KCNE1</i>
			MiRP1	<i>KCNE2</i>
Pacemaker current	-	<i>HCN2</i>		
	-	<i>HCN4</i>		
$I_{\text{K1}}$	Kir2.1	<i>KCNJ2</i>	SUR2	<i>ABCC9</i>
	Kir2.2	<i>KCNJ12</i>		
$I_{\text{K-ATP}}$	Kir6.1	<i>KCNJ8</i>		
	Kir6.2	<i>KCNJ11</i>		
$I_{\text{K-Ach}}$	Kir3.1	<i>KCNJ3</i>		
	Kir3.4	<i>KCNJ5</i>		

The other important inward current is the  $\text{Ca}^{2+}$  influx conducted by sarcolemmal voltage-gated  $\text{Ca}^{2+}$  channels ( $I_{\text{Ca}}$ , Figure 4).  $I_{\text{Ca}}$  is produced by two different types of voltage-gated  $\text{Ca}^{2+}$  channels that are distinguished by their electrophysiological properties (71). The so-called T-type  $\text{Ca}^{2+}$  channels activate in the relatively hyperpolarized membrane and inactivate very fast. T-type  $\text{Ca}^{2+}$  channels are thought to contribute to pacemaker activity in the SAN and in the AVN. The second type of cardiac voltage gated  $\text{Ca}^{2+}$  channels is the L-type  $\text{Ca}^{2+}$



channels. It plays a role in maintaining the characteristic long lasting plateau phase of the cardiac action potential and in excitation conduction coupling. Both the T-type and the L-type channels are encoded by the *CACNAI* gene family. The *CACNAI* gene family contains 10 members called *CACNA1A* to *CACNA1S*. T-type and L-type channels are encoded by the *CACNA1H* and *CACNA1C* genes, respectively (Table 1).

Contrary to the inward currents, determining the molecular features of the cardiac outward, mainly  $K^+$  currents is much more challenging. The  $K^+$  channels show the largest functional and structural diversity among the ion channels. According to their function, the  $K^+$  channels may be classified as  $I_{to}$ ,  $I_{Kur}$ ,  $I_K$  and  $I_{K1}$  channels (Figure 4). On the other hand, there are approximately one hundred  $K^+$  channel coding subunit genes in the human genome (15) and it appears that at least half of them are expressed in the heart. Furthermore, there are strong evidences showing that different  $K^+$  channel subunits may co-assemble in channel complexes, further increasing the possible functional heterogeneity. Moreover, there are auxiliary subunits that may join to various channel complexes modulating channel function. The co-assembly of channel subunits and the existence of the auxiliary subunits in the heart muscle raise the number of theoretical combinations to almost infinite.

According to the Gene Nomenclature Committee of the Human Genome Organization most of the  $K^+$  channel subunit coding genes belong to the *KCN* gene family. However, there is an alternative and widely used nomenclature. According to the latter, the six transmembrane domain subunits are denoted as  $KvN.N$  ('v' for voltage gated) and the two transmembrane domain subunits as  $KirN.N$  ('ir' for inwardly rectifying) where 'N'-s stand for numbers showing the number of the subfamily and the number of the member in the subfamily, respectively.

The known molecular bases of cardiac ion currents (45) are summarized in Table 1 including two  $K^+$  channel types that have not been mentioned previously: the  $I_{K-ATP}$  and the  $I_{K-Ach}$  channels. Both of them conduct repolarizing  $K^+$  currents and are built up by two transmembrane domain subunits (Figure 7). In the ventricles  $I_{K-ATP}$  channels are located in the cell membrane, in the inner membrane of the mitochondria, as well as in the nuclear envelope (83). They provide a link between cellular metabolism and the electrical activity of the heart muscle cells since they are inhibited by ATP and opened by nucleotide diphosphates. Opening of  $I_{K-ATP}$  channels is an important cellular response under hypoxic conditions and results in shortening of action potential durations and minimizing  $K^+$  efflux. They are most likely involved in ischemic preconditioning of the heart. Mitochondrial  $I_{K-ATP}$  channels are thought to help in maintaining the mitochondrial matrix volume in high-work states of the heart.  $I_{K-Ach}$

channels are primarily present in the pacemaker regions of the heart (31). They are gated by a G protein-coupled mechanism mediated by muscarinic acetylcholine receptor. Acetylcholine is released on the axon termini of nervus vagus and mediates parasympathetic effects. Following the activation of the acetylcholine receptors, the opening of the  $I_{K-Ach}$  channels results in a decrease of the pacemaker potential and slows down the heartbeat rate.

### **Channel disorders**

Because heartbeat depends on the proper streaming of ions through the cell membrane during the heart cycle, disorders of ion channels play key roles in cardiac diseases. Ion channel diseases may result in disturbances of normal heart rhythm. When heart beats are too slow (bradycardia), or are so rapid that the heart can not be filled up with blood properly (tachycardia), circulatory collapse or heart failure may occur.

Ventricular tachycardia and ventricular fibrillation are the most serious and frequent consequences of many cardiac ion channel disorders. The mechanism of ventricular fibrillation is unclear, however, abnormal repolarization that results in elongated action potential duration is likely to play a role. The archetypical repolarization disease is called the long-QT syndrome since the elongated action potential appears as an expanded QT interval in the ECG. An elongated QT interval does not necessary result in abnormal heart rhythm; however, patients affected by long-QT syndrome are predisposed to ventricular tachyarrhythmias that may lead to sudden heart failure and death (61).

There are inherited and acquired types of long-QT syndrome. The heritable form is caused by mutations in ion channel genes and is inherited as autosomal dominant or autosomal recessive mutations (14). The more frequent dominant form is caused by gain of function mutations in the  $Na^+$  channel genes or by loss of function mutations in one of the four  $I_K$  channel subunit coding genes (Table 2). The gain of function mutant  $Na^+$  channels fail to become inactivated and thus drive an excess inward current during the plateau phase of the action potential, which leads to disruption in the balance between inward and outward currents resulting in delayed repolarization and prolonged action potential duration. In contrast, the long-QT causing  $K^+$  channel mutant alleles are of dominant negative types that decrease  $I_{Kr}$  or  $I_{Ks}$ . The weaker repolarizing currents expand the action potential. The dominant negative effect of the above mutations may be explained by the fact that  $I_K$  channels are assembled from four subunits (Figure 7). Incorporation of a dominant negative mutant subunit changes the structure of the channel complex in a way that it results in a decreased ion conductance.

In addition to the dominant ones recessive mutations have also been reported to cause QT interval elongation. In patients homozygous for the far less frequent long-QT causing recessive alleles the slow component of  $I_K$  ( $I_{Ks}$ , Table 1 and 2) is absent. Such patients also suffer from congenital deafness due to lack of endolymph in the inner ear. Studies motivated by such individuals led to the recognition that  $I_{Ks}$  may be necessary for the endolymph production in the inner ear.

Several of the long-QT patients possess no clinical syndromes and go undetected. They are predisposed not only to eventual ventricular arrhythmias but also to effects of a number of extracardial medications including antibiotics, antidepressants or appetite suppressants. Many of these medicines have been shown to elongate QT interval by selectively blocking  $I_{Kr}$  channels (43). It is very likely that there is a repolarization reserve built in the large variability in the  $K^+$  channels that is able to compensate the effects of some long-QT causing mutations. However, chemical block of repolarizing channels together with the effect of mutations may lead to the depletion of the repolarization reserve and to unexpected sudden cardiac death because of serious arrhythmias (60).

**Table 2.** Genes affected by mutations that cause inherited long QT syndrome. The autosomal dominant and the autosomal recessive forms are often called Romano-Ward and Jervell-Lange-Nielsen syndrome, respectively.

Gene	Current
Autosomal dominant (Romano-Ward)	
KvLQT1 ( <i>KCNQ1</i> )	$I_{Ks}$
HERG ( <i>KCNH2</i> )	$I_{Kr}$
<i>SCN5A</i>	$I_{Na}$
minK ( <i>KCNE1</i> )	$I_{Ks}$
MiRP1 ( <i>KCNE2</i> )	$I_{Kr}$
Autosomal recessive (Jervell-Lange-Nielsen)	
KvLQT1 ( <i>KCNQ1</i> )	$I_{Ks}$
minK ( <i>KCNE1</i> )	$I_{Ks}$

Studies on heritable forms of long-QT syndrome provided important insights into the pathophysiology of a far more frequent cardiac disease: heart failure (39). Heart failure represents the common consequence of many pathological processes like atherosclerosis, hypertension or viral infections. Regardless of the initiating factors the common phenotype is a dilated, poorly contracting heart. The affected patients suffer from decreased ability to exercise and shortness of breath. It has been shown that in heart failure the repolarizing  $K^+$

currents are downregulated, which results in prolonged action potentials (7). Longer action potentials are adaptive in short term, because a longer plateau phase means more time available for excitation-contraction coupling which may compensate the inadequate pump function of the heart. However, longer action potential durations are maladaptive in long term since – similarly to the long-QT syndrome – they increase the risk of fatal ventricular arrhythmias.

In addition to the extension of the QT interval, shorter action potentials may also result in abnormalities in the heart rhythm through a slightly different mechanism. Certain mutations result in faster than normal inactivation of the  $\text{Na}^+$  channels. This  $\text{Na}^+$  channel dysfunction results in insufficient depolarization that may appear in the form of shortened action potentials. However, action potential shortening is most dramatic in those regions where the phase 1 transient  $\text{K}^+$  current ( $I_{\text{to}}$ , Figure 4) is more prominent than in the adjacent regions, like in the epicardial layer of the ventricular wall compared to the inner layers (Figure 6). Due to the shorter action potentials in the epicardium the inner layers may re-excite the prematurely repolarized epicardial cells leading to idiopathic ventricular fibrillation, another frequent cause of unexpected sudden cardiac death (12).

### **Viral gene transfer into cardiomyocytes**

The conventional ways of introducing genes into cells, such as calcium phosphate transfections and liposome- or lipofectamine-mediated methods, work poorly in primary cultures of adult cardiomyocytes and are of little value when genes need to be introduced into a large number of cardiac cells. Viral vectors, however, can be used to achieve this goal. In the past decades, several different viral gene transfer systems have been developed and most of them have been tested in cardiomyocytes. Type 5 adenoviruses work well in cardiomyocytes, but they are challenging to produce, and moreover, their immunogenicity prevents their use in long-term *in vivo* experiments (25). The adeno-associated virus is suitable for *in vivo* myocardial gene transduction because of its low or absent immunogenic potential (25), but its use for *in vitro* studies is limited by the low gene expression achieved in cardiomyocytes (73). According to our knowledge, the herpes viruses have not been suggested to use for gene transfer into cardiomyocytes. However, given the fact that herpes viruses are known to efficiently infect post-mitotic cells and considering our promising preliminary results on successful infections with a herpes virus into cardiomyocytes, the potential of herpes viruses for cardiac gene transfer *in vitro* and potentially *in vivo* is undeniable. In our second project the main objective was the development of an efficient herpes-virus-based-vector and the assessment of its capabilities in delivering genes into

ventricular cardiomyocytes. We chose to use the Pseudorabies virus, of which molecular biology is one of the best known ones among herpesviruses. In addition, in our third project, encouraged by recent reports on successful infections of cardiomyocytes by lentivirus vectors, we applied a lentivirus-based system to deliver artificial microRNAs to induce RNA interference thereby in atrial cardiomyocytes.

### ***The Pseudorabies virus***

Pseudorabies virus (PRV) is present and affects many aspects of our life. PRV is the causative agent of Aujeszky's disease in swine. Causing destructive disease and economic losses worldwide, PRV is of primary importance for those who are concerned about disease control in swine agriculture. PRV has served as a model organism for the study of molecular biology of herpesviruses. The virus is also being used as a tracer of neuronal pathways, making use of its remarkable ability to infect synaptically connected neurons (reviewed in 19).

Based on its broad host range, its rapid rate replication to produce new virus particles in a matter of hours accompanied by strong cytopathic effects and based on its ability to establish life-long infections in the sensory ganglia, PRV is classified into the Alphaherpesvirinae subfamily and into the Varicellovirus genus of herpesviruses. Like all herpesviruses, the PRV virion has a double stranded DNA genome enclosed in an icosahedral capsid. The capsid is surrounded by tegument proteins which are organized into two layers, one which interacts with the capsid and one which interacts with the envelope. The envelope, the outmost layer of the PRV virion is a lipid bilayer infused with transmembrane proteins. The life cycle of a herpesvirus consists of two main stages. While the *lytic cycle* has strong cytotoxic effects and results in the generation of new virions, in *latency*, the virus resides in rest in the nucleus of the host cell throughout the lifetime of the infected cell or until the virus returns into the lytic cycle in the course of a reactivation process. During the virion entry, the envelope fuses with the cell membrane and the capsid, together with the tegument proteins, is released into the cytoplasm. The tegument proteins interact with the protein synthesis machinery of the host cell immediately after entering the cell. The capsid is transported along the microtubules to the nucleus. Upon arrival to the nucleus, the only immediate early protein of PRV (*IE180*, Figure 10) is transcribed by RNA polymerase II and a transcriptional cascade begins. The IE180 protein is a transcriptional transactivator, it initiates transcription of early genes. Some early genes, such as *EP0* (Figure 10), act as transactivators and others are involved in the replication of viral DNA. Viral DNA is replicated by a rolling-circle mechanism. The onset of viral DNA replication signals the production of late proteins, including capsid proteins. The capsid is assembled in the nucleus and the virus genome is packed into the capsid. The fully

assembled capsid buds out of the nucleus into the cytoplasm, where it associates with tegument and envelope proteins. The virion gains its final envelope by budding into the trans-Golgi apparatus and finally, the mature virion is transported to the cell surface within a sorting vesicle. In latency, however, only a small portion of the virus genome is transcribed, resulting in the so-called latency associated transcripts (LATs, LLT and LRT, Figure 10). LATs are transcribed from the opposite strand of the *IE180* and *EP0* genes and are thought to negatively regulate their expression (56).

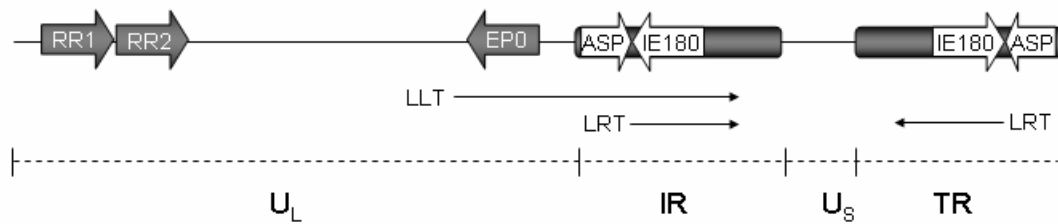


**Figure 10.** Schematic illustration of the PRV genome. RR1 and RR2 are open reading frames for the large and small subunits of ribonucleotide reductase. EP0 encodes early protein 0. ASP shows location and orientation of the latency associated antisens promoter, which mediates expression of LRT. IE180 encodes the immediate early protein 180. LLT and LRT stand for large latency associated transcript and latency related transcript, respectively. The scale bar in the bottom shows the main structural landmarks of the PR genome ( $U_L$ : long unique, IR: internal repeat,  $U_S$ : short unique, TR: terminal repeat).

### ***Lentivirus vectors***

Lentiviruses are classified into the *Lentivirinae* genus of retroviruses. Retroviruses are dependent on the host cell undergoing mitosis for the integration of the viral DNA with the host genomic DNA. Unlike other retroviruses, lentiviruses can enter the nucleus even without mitosis. This unique ability of lentiviruses among retroviruses makes them an ideal choice for delivering genetic material into growth-arrested cell types, such as cardiomyocytes. In the past decade, lentivirus-based gene transfer vectors have been developed from feline, simian, equine and human lentiviruses (80). Based on our massive and increasing knowledge on the molecular biology of the human lentivirus Human immunodeficiency virus type 1 (HIV-1), HIV-derived lentivirus vectors have evolved to be superior over vectors developed from viruses of other species.

HIV-1 is the etiologic agent of the acquired immunodeficiency syndrome (AIDS), a condition in which the immune system begins to fail leading to increased susceptibility for life-threatening opportunistic infections. HIV-1 primarily infects leukocytes such as helper T cells (specifically CD4 positive T cells), macrophages and dendritic cells. HIV-1 infection leads to low levels of CD4<sup>+</sup> T cells through three main mechanisms: direct viral killing of

infected cells, increased rates of apoptosis in infected cells and killing of infected CD4<sup>+</sup> T cells by CD8<sup>+</sup> cytotoxic T cells that recognize infected cells. When CD4<sup>+</sup> T cell numbers decline below a critical level, cell-mediated immunity is lost, and the body becomes progressively more susceptible to opportunistic infections.

The HIV-1 virion carries two copies of the single-stranded RNA genome, packed in a truncated cone-shaped nucleocapsid. Together with the RNA genome, several different enzymes, such as reverse transcriptase, protease, ribonuclease and integrase are packed in the nucleocapsid. The nucleocapsid is surrounded by the matrix, which is composed of the viral matrix protein and which ensures the integrity of the nucleocapsid. The matrix, in turn, is surrounded by the envelope, a phospholipid bilayer, in which the hexameric envelop glycoprotein complexes are embedded. The envelop complexes, which can interact with the CD4 glycoprotein and with one of the co-receptors (usually CXCR4 or CCR5 chemokine receptors) on the surface of the leukocytes, are responsible for the tropism of the virus.

The HIV genome is extremely compact and has complicated structures. HIV has three structural and six accessory genes encoding altogether 19 proteins. During the production of viral proteins, the primary RNA transcript is multiply spliced, the spliced mRNAs are alternatively translated by the differential usage of overlapping reading frames and the primary protein precursors are further processed by proteolytic enzymes. The three structural genes encode viral proteins. *Gag* encodes matrix, capsid and nucleocapsid proteins, *pol* encodes three proteins that have enzymatic activities (reverse transcriptase, protease and integrase) and *env* carries information for the production of the two subunits of the envelope protein complex. The six accessory genes are regulatory genes that control expression of viral proteins (*tat* and *rev*) or interact with host cell processes (*nef*, *vif*, *vpr*, and *vpu*) determining virulence, pathogenicity of the virus (77).

During the development of modern HIV-based lentivectors, measures have been made to ensure biosafety and broad host range of the vector and the long-term expression of the transgene that is to be delivered into the target cells. Accessory genes which are not required for the generation of the vector or for a successful transduction, such as *nef*, *vif*, *vpr* and *vpu*, have been deleted from the HIV genome (Figure 11 A). The remaining genome has been split into three parts and has been engineered to be carried by three bacterial plasmids, which are often called packaging plasmids, allowing easy manipulation and production. One plasmid carries structural genes (*gag* and *pol*) and genes that transactivate either viral protein production or the transcription of the virus RNA genome during vector production (*rev* and *tat*). Another plasmid carries the gene encoding the envelope protein. In most of the cases,

instead of the *env* gene of HIV, pseudotyped lentivirus vectors are produced by using the envelope protein G of the Vesicular stomatitis virus (VSV-G). Pseudotyping by the VSV-G protein has two main advantages. Firstly, it confers the broad host range of VSV to the lentivirus vector. Secondly, the VSV-G pseudotyped lentivirus vector can withstand the shearing forces that are generated during ultracentrifugation, allowing the production and purification of high-titer virus stocks. The third plasmid, the so-called vector plasmid, in addition to the transgene, carries essential structural landmarks of the HIV genome, such as the packaging signal and the long terminal repeats (LTRs). The packaging signal is indispensable in the assembly of the virus capsid during production of new virions. LTRs have multiple functions. They govern replication of the virus genome by transcription, initiate reverse transcription during transduction and play a role when the virus genome is inserted into the genome of the host cell. Self-inactivating lentivectors have been developed by introducing a deletion in the 3' LTR, resulting in the loss of promoter function (SIN-LTR, Figure 11 B). During the vector production, the intact 5' LTR promotes transcription of the vector genome. When the vector genome is reverse transcribed in the host cell, however, the 5' LTR is replaced by the SIN-LTR which is no longer able to initiate transcription of the virus genome. Hence, the vector that is incorporated into the genome of the infected cell remains silent, only the transgene remains transcriptionally active. In the case of the so-called advanced generation of the lentivectors, two cis-acting elements, the so-called central polypurine tract (cPPT) of the HIV *pol* gene and a posttranscriptional regulatory element of the Woodchuck hepatitis virus (WPRE) have been added to the vector. These additions have been shown to enhance transduction efficiencies under various conditions (11).

Lentivectors are generated by introducing a mixture of the three packaging plasmids into the producer cells by calcium-phosphate or liposome mediated transfection. Most commonly Hek 293 cells are used for this purpose. Newly formed virus particles are harvested from the culture medium in the following 24-48h after transfection. Under these conditions, all essential structural proteins are provided *in trans* in the producer cells. However, only RNA molecules that are transcribed from the vector plasmid carrying the packaging signal are packed into the newly formed virions. Therefore, no viral protein-coding genes are introduced by the vector into the target cells during transduction, which greatly enhances biosafety by minimizing chances for the formation of replication-competent vectors (Figure 11 B).



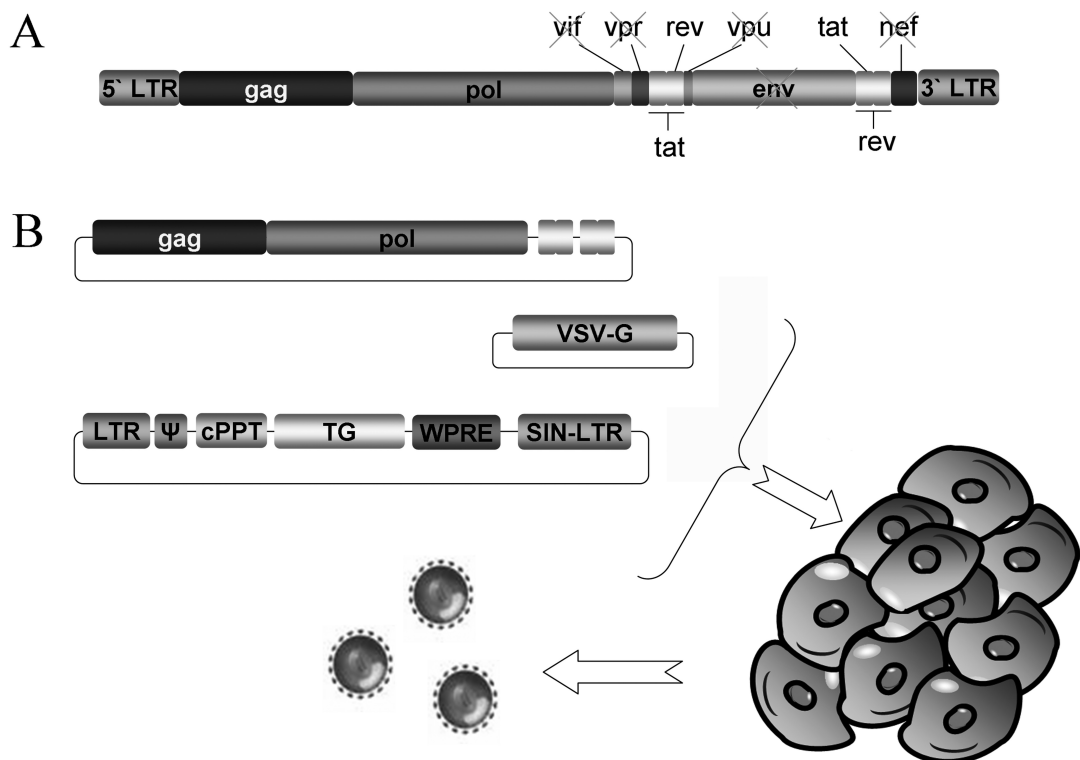


**Figure 11. A:** Genetic map of the HIV-1 genome. In the multiply attenuated lentiviral vectors five genes which contribute to the virulence and pathogenicity of HIV-1 are deleted. **B:** Working schema of lentivirus vector production. The packaging plasmids are co-transfected into Hek293 cells. Lentivirus particles are harvested from the supernatant of the culture medium.

### RNA interference

RNA interference (RNAi) is a biological response to double-stranded RNA and is highly conserved in many organisms from yeast to human. RNAi mediates resistance to both endogenous parasitic and exogenous pathogenic nucleic acids, and regulates the expression of protein-coding genes. RNAi has become a powerful research tool for probing gene function by manipulating gene expression experimentally, and it has promising potential in biotechnology and medicine as well.

The two types of RNA molecules that play central role in the RNAi pathway are small interfering RNA (siRNA) and microRNA (miRNA) (28). siRNAs are 21-25 nucleotide long double-stranded RNAs (dsRNAs) with 3' dinucleotide overhangs and complete complementarity between the two strands. siRNAs are produced from relatively long dsRNAs through the action of the RNase III enzyme Dicer (Figure 12). Dicer recognizes dsRNA

substrates from many different sources. Viruses, transposons, experimentally introduced dsRNAs or endogenously expressed dsRNAs generated by bi-directional transcription are ultimately processed by Dicer. siRNAs operate in large ribonucleoprotein complexes termed RNA induced silencing complex (RISC). During RISC assembly, the double-stranded siRNA is unwound to incorporate only a single-stranded RNA molecule in the final active complex. Once assembled, siRNA-RISC recognizes and cleaves mRNAs complementary to the incorporated single-stranded siRNA.

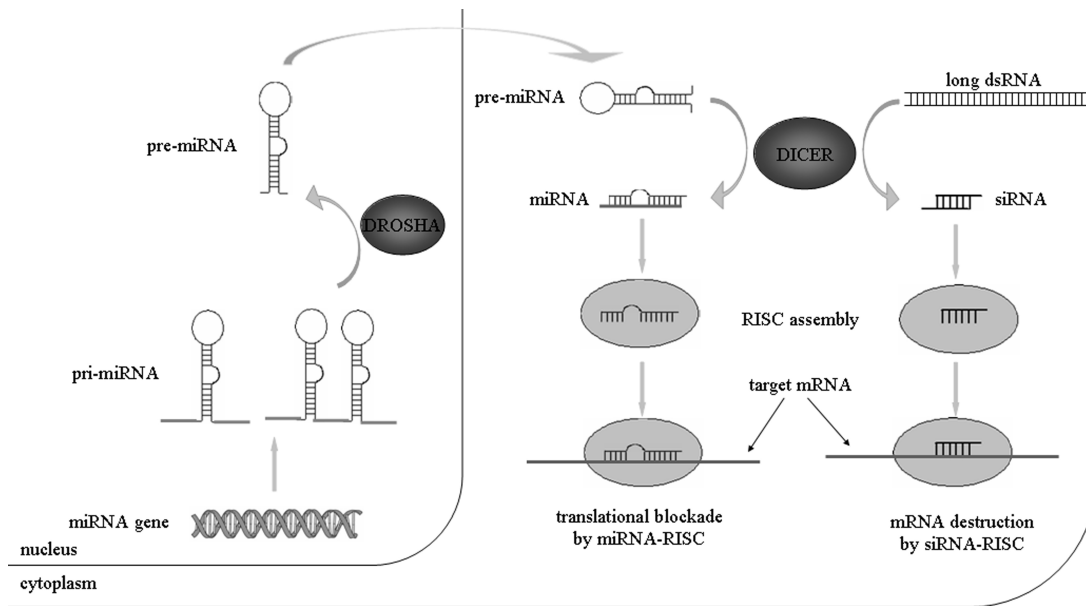


**Figure 12.** The RNAi pathway.

miRNAs, however, are derived from larger precursors that form characteristic imperfect stem-loop hairpin structures (pri-miRNA, Figure 12). Some miRNA genes are located in introns and some of them are clustered in polycistronic transcripts encoding two or more different miRNAs. The mature miRNA is released from the primary transcript through a stepwise processing by two RNase III enzymes: Drosha, which acts in the nucleus and Dicer, which acts in the cytoplasm. One strand of the mature miRNA, the so-called guide strand, similarly to the siRNAs, is incorporated into the RISC complex. The miRNA-RISC complex binds to the complementary mRNAs. miRNAs usually have binding sites in the 3' UTR of the target mRNAs and function as translational repressors.

RNAi can be induced experimentally by several different ways. RNAi triggered by long dsRNA has been successfully used in *Caenorhabditis elegans* or in *Drosophila melanogaster*. Long dsRNA, however, is toxic for mammalian cells, possibly due to the activation of antiviral responses. In these cell types siRNAs, which are generated by *in vitro* DICER

cleavage or which are synthesized *in vitro*, can be used. Optionally, siRNAs could be genetically encoded in the form of a small hairpin RNA (shRNA). shRNAs have similar stem-loop structure to a pre-miRNA, but unlike miRNAs, they are fully complementary to their target mRNA. shRNAs are expressed from RNA polymerase III promoters, such as U6 or H1. The shRNA technology has recently been further improved by the development of miRNA-based shRNAs, the so-called shRNAmirs (72). shRNAmirs utilize the complete RNAi pathway by expressing a full-length pri-miRNA, in which the miRNA sequence has been replaced by the sequence of an siRNA complementary to the selected target mRNA (Figure 13 A). shRNAmirs can be expressed from RNA polymerase II promoters. Therefore, in addition to the greater knock-down efficiency, the shRNAmir system offers higher compatibility to the most frequently used vector systems, including those that allow regulated expression of the transgenes. shRNAmirs can also be used in combination with viral gene delivery systems. The genetic map of a lentivirus vector overexpressing a shRNAmir gene is shown in Figure 13 B.

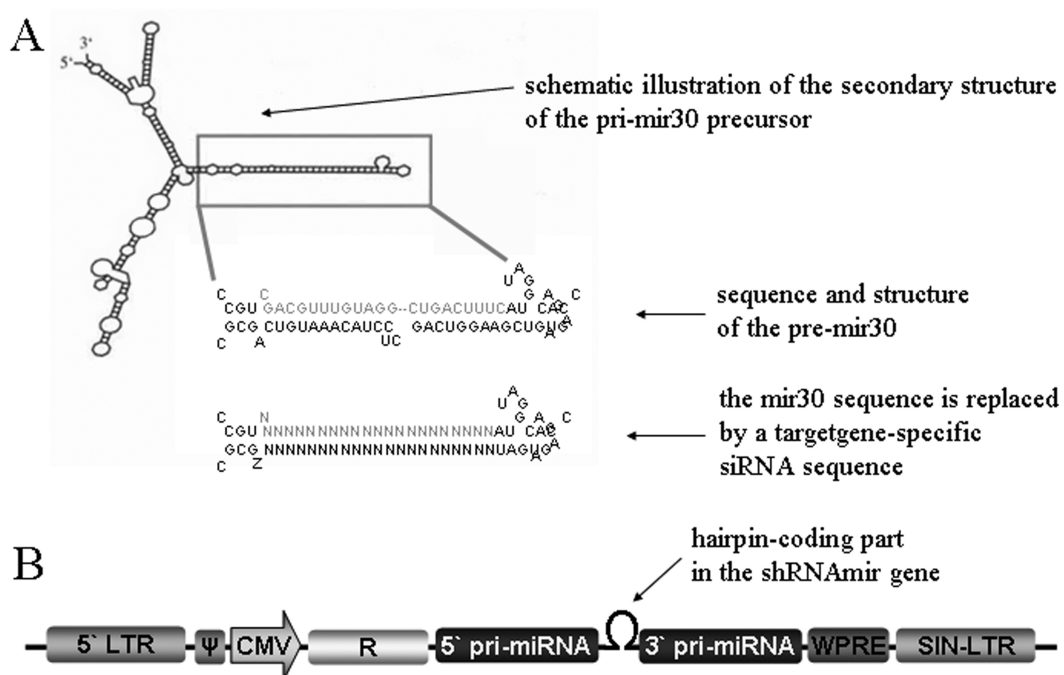


**Figure 13. A:** Schematic illustration of the general concept of shRNAmirs. In upper left the predicted structure of the mir30 precursor is shown. In shRNAmirs, the mir30-coding hairpin is replaced by a target gene-specific siRNA. **B:** Genetic map of shRNAmir expressing lentivectors. The shRNAmir is encoded in the 3' UTR of a reporter gene (R).

## **Materials and Methods**

### **Tissue samples**

Human heart tissue samples (approximately 100–150 mg for each sample) were isolated from 19 undiseased human donor hearts. The hearts were isolated from organ donor patients (Appendix) through pulmonary and aortic valve transplantation surgery. Before the explantation of the hearts, the patients did not receive any medication. Before preparation, the hearts were perfused with cardioplegic solution and were kept cool (4–6°C) for 6–8 h. Cross sections of the ventricle and atrial walls were excised and frozen in liquid nitrogen. The protocol conforms to the principles outlined in the Declaration of World Medical Association proclaimed in Helsinki (Cardiovascular Research 1997; 35: 2–4) and was approved by the Ethical Review Board of University of Szeged (No.51–57/1997 OEj.).

### **Atrial cardiomyocyte and cardiac fibroblast isolation**

Canine atrial cardiomyocytes and cardiac fibroblasts were isolated by previously described methods (82). All animal care procedures followed NIH guidelines and were approved by the Animal Research Ethics Committee of the Montreal Heart Institute. Adult mongrel dogs (20–30 kg) were anesthetized with morphine (2 mg/kg s.c.) and  $\alpha$ -chloralose (120 mg/kg i.v.) and mechanically ventilated. The heart was removed after intra-atrial injection of heparin (10,000 U), immersed in 2 mmol/L  $\text{Ca}^{2+}$ -containing Tyrode's solution. The left coronary artery was cannulated and left-atrial tissue was perfused with Tyrode's solution (37°C, 100% O<sub>2</sub>), then with  $\text{Ca}^{2+}$ -free Tyrode's solution (~5 minutes), followed by ~40-minute perfusion with the same solution containing collagenase (~0.4 mg/mL, CLSII, Worthington) and 0.1% bovine serum albumin (BSA, Sigma). Tissue was minced and the cells were kept in medium-199. Cardiomyocytes were pelleted by centrifugation at 500 rpm (1 min) and cardiac fibroblasts were harvested from the supernatant. Cardiomyocytes were plated on laminin precoated coverslips in M199 medium (Invitrogen). Cardiac fibroblasts were plated in T25 tissue culture flasks in DMEM medium (Invitrogen), supplemented with 10% fetal calf serum (FCS, Gibco).

### **Ventricular cardiomyocyte isolation**

All experiments were conducted in compliance with the NIH guidelines and were approved by the review board of the Committee on Animal Research of the Albert Szent-Györgyi Medical University. The modified protocol for cell isolation was based on established procedures described earlier in details (75). Canine ventricular myocytes were enzymatically

dissociated as follows. A portion of the left ventricular wall containing an arterial branch large enough to cannulate was perfused in a modified Langendorff apparatus with solutions in the following sequence: (1) normal Tyrode's solution (10 minutes), (2)  $\text{Ca}^{2+}$ -free Tyrode solution (10 minutes), and (3)  $\text{Ca}^{2+}$ -free Tyrode solution containing collagenase (type I, 0.66mg/mL) and bovine serum albumin (fraction V, fatty acid free, 2mg/mL) (15 minutes). Protease (type XIV, 0.12mg/mL) was added to the final perfusate while a further 15–30 minutes long digestion was allowed. Freshly dissociated cardiomyocytes were pelleted at 50g and resuspended in sterile solution five times.  $\text{Ca}^{2+}$  concentration was increased step-wise to 1mM. After the last centrifugation cardiomyocytes were resuspended in M199 medium (Sigma), supplemented with 5mM creatine, 2mM L-carnitine, 5mM taurine and 100 units/mL insulin. Cells were plated on laminin precoated coverslips.

### **Whole-cell patch clamp**

Whole-cell patch-clamp technique (voltage-clamp mode) was applied for characterizing macroscopic  $I_{\text{to}}$  parameters in control and transduced atrial cardiomyocytes. All experiments were performed at  $36 \pm 0.5^\circ\text{C}$ . Borosilicate-glass electrodes had tip resistances between 1.5 and 3.0  $\text{M}\Omega$  when filled. Cell capacitance and series resistance were compensated by ~80% to 90% to minimize the capacitive surge on the voltage recording. Leakage compensation was not used. Cell capacitances were not different between experimental groups. The standard Tyrode solution contained (in mmol/L) NaCl 136, KCl 5.4,  $\text{MgCl}_2$  1,  $\text{CaCl}_2$  1,  $\text{NaH}_2\text{PO}_4$  0.33, HEPES 5 and dextrose 10 (pH 7.35 with NaOH). The high- $\text{K}^+$  storage solution contained (in mmol/L) KCl 20,  $\text{KH}_2\text{PO}_4$  10, dextrose 10, mannitol 40, L-glutamic acid 70,  $\beta$ -OH-butyric acid 10, taurine 20, EGTA 10 and 0.1% BSA (pH 7.3 with KOH). The standard pipette solution contained (in mmol/L) K-aspartate 110, KCl 20,  $\text{MgCl}_2$  1, MgATP 5, GTP 0.1, HEPES 10, Na-phosphocreatine 5, EGTA 5 with pH adjusted to 7.3 with KOH. Atropine (1- $\mu\text{mol/L}$ ),  $\text{CdCl}_2$  (200- $\mu\text{mol/L}$ ) and tetraethylammonium chloride (10mmol/L) were added to the external solutions to eliminate muscarinic  $\text{K}^+$ -currents, to block  $I_{\text{Ca}}$  and  $I_{\text{Kur}}$ , respectively.  $I_{\text{Na}}$  contamination was avoided by using a holding potential at -50 mV.

### **Generation of recombinant PRV strains**

Different PRV strains were propagated on subconfluent monolayer of porcine kidney (PK-15) cells. PK-15 cells were grown in DMEM (Sigma) supplemented with 5% FCS (Gibco). PRV was harvested from the supernatant of PK-15 cells infected by the virus at 1 m. o. i. 24 hours post-infection.

Recombinant PRV strains were generated in PK-15 cells by site-directed insertional mutagenesis. PK-15 cells were co-transfected with the purified DNA of the parent virus and a targeting plasmid. The targeting plasmid, in general, carries a reporter gene flanked by viral sequences. The viral sequences flanking the reporter gene are homologous to the genomic region where the reporter gene is to be introduced. The homologous sequences in the targeting plasmid and the viral genome allow double homologous recombination, which results in a recombinant virus genome. By careful targeting plasmid design a deletion can be introduced at the same time, compensating for the possible negative effects of an enlarged genome size on virus propagation.

The construction of the basic targeting plasmids has been described previously. The targeting plasmid for the ribonucleotide reductase (RR) gene carries a genomic fragment of PRV overlapping the open reading frames of the large (RR1) and the small (RR2) subunits of the RR enzyme (9). A deletion, including 1789 bp of the RR1 and 7 bp of the RR2 open reading frames was generated in this plasmid. The *EP0* gene targeting plasmid carries a PRV genomic fragment homologous to the *EP0* gene and a deletion affecting 1390 bps overlapping with the *EP0* open reading frame (8). The third targeting plasmid used in this study carries a viral genomic fragment homologous to the latency associated putative antisense promoter (ASP) (10). An EcoRI site was inserted into the TATA box of ASP, abolishing promoter function of ASP and allowing subcloning of reporter genes (*lacZ*, *gfp*, *cameleon* or *troponeon*).

### **Generation of shRNAmir expressing lentivectors**

shRNAmir oligo sequences for the canine KCNE3 mRNA were designed by the web-based 'shRNA retriever' tool available on the homepage of Ravi Sachidanandam's laboratory (<http://katahdin.cshl.org/>, Cold Spring Harbor Laboratory, NY, USA). During the entire procedure for cloning shRNAmirs, previously published protocols have been followed (50). Synthetic single-stranded shRNAmir oligonucleotides were PCR amplified and cloned directly in a modified version of pGIPZ lentivirus vector plasmid (Openbiosystems), in which the EcoRI site at position 5394 has been removed by partial EcoRI digestion, Klenow fill-in of 3' overhanging DNA ends and re-circularization.

Protocols for the generation of lentiviruses and the lentivirus packaging plasmids (psPAX2 and pMD2.G) were obtained from Didier Trono's laboratory (<http://tronolab.epfl.ch/>, Ecole Polytechnique Federale de Lausanne, Lausanne, Switzerland). The vector and packaging plasmids were amplified in *E. coli* DH5 $\alpha$  and purified by Nucleobond anion exchange columns (Macherey-Nagel) following the manufacturer's instructions. The Hek293T/17 cell

line used for lentivirus production was obtained from ATCC (Manassas, VA, USA) and were grown in DMEM (Invitrogen) supplemented with 10% FCS. Lentiviruses were produced as it is briefly summarized below. A subconfluent monolayer of Hek293T/17 cells was transfected with a plasmid mixture containing the pGIPZ-shRNA<sub>mir</sub> vector, the psPAX2 and pMD2.G packaging plasmids in a 2:2:1 weight ratio, respectively, by the calcium-phosphate precipitation method. 12-14 hours after transfection, the culture medium was replaced by fresh DMEM supplemented with 10% FCS. The conditioned medium was harvested 36-48 hours post-transfection. The harvested medium was clarified from cell debris by filtration using a 0.45µm pore size syringe-attachable filter. For cardiac fibroblast infections, the filtered medium containing virus particles was either kept at +4°C for short term or kept frozen in aliquots at -80°C for long term use. For cardiomyocyte infections virus particles were precipitated by ultracentrifugation, re-dissolved in sterile PBS supplemented with 10% BSA and stored at -80°C in aliquots.

### **Gene expression profiling in human cardiac tissue samples**

Crude total RNA extracts from fresh or frozen tissues were obtained by following a protocol described by Gauthier et al (22). RNA samples were further purified by using Nucleospin RNA II kit (Macherey-Nagel), as recommended by the manufacturer. The concentration of total RNA samples was determined by UV-photometry.

Reverse transcription (RT) was performed by using Superscript II RNase H<sup>-</sup> Reverse Transcriptase (Invitrogen). Each RT reaction mixture contained 5 µg total RNA, 200 U reverse transcriptase and 100 pmol dT<sub>(15)</sub> oligonucleotide at a final volume of 20 µl. Nine micro liters of the diluted RT products (corresponding to 56.25 ng total RNA equivalent) were used for each real-time RT-PCR assay. RNA samples were tested for the presence of genomic DNA contamination by running no-RT control reactions. Gene-specific primers were designed using the Primer Express software (Applied Biosystems) according to the software guidelines. Where splice variants were known, primers were designed in the invariable regions of mRNA splice alternatives. For primer sequences, see the online supplementary data in ref. 48). SYBR-Green PCR assays were performed on a Rotor-Gene 3000 (Corbett Research) real-time PCR platform. For each 20 µl reaction, 9 µl cDNA solution, 10 µl Absolute QPCR SYBR Green Mix (ABgene), 0.5 µl forward primer (10 µM) and 0.5 µl reverse primer (10 µM) were mixed together. To assess primer dimer formation, blank controls containing water as template were used for every primer pairs in each experiment. PCR parameters were as follows: 95°C, 15 min for heat activation of DNA polymerase, followed by 94°C, 25 s (denaturation), 61°C, 25 s (annealing) and 72°C, 15 s (synthesis) for

50 cycles. After each run a melting point analysis was performed by measuring fluorescence intensity in a temperature interval ranging from 55 to 93°C. Samples showing abnormal melting point characteristics were excluded from analysis.

In a typical experiment expression levels of eight ion channel genes were analyzed along with  $\beta$ -actin as internal control. We calculated the relative copy numbers by normalizing each ion channel-coding mRNAs to  $\beta$ -actin using the 'Comparative Quantitation' module of the Rotor-Gene software (version 6.0, Corbett Research).

Based on the results of initial experiments we assumed that  $\beta$ -actin is stably expressed in both regions of the human heart analyzed in this study. To validate this hypothesis we compared the expression level of  $\beta$ -actin in the two regions of the heart. We constructed an external standard curve from a dilution series of a synthesized  $\beta$ -actin template. *CP* values of  $\beta$ -actin from ventricular and from atrial cDNAs were compared to the standard curve. We found that  $\beta$ -actin was 1.7-times more abundant in the left ventricle than in the left atrium. Hence, for a reliable comparison of gene expression levels in the ventricle with those in the atrium, we corrected the atrium related data by dividing the mean of the relative copy number of each mRNA by 1.7. Statistical analyses were performed using Student's t-test and significance was set at  $P < 0.05$ .

### **Validating MiRP2 knock-down in cardiac fibroblasts**

Isolated canine atrial fibroblasts were plated in T-75 culture flasks in DMEM (Invitrogen) supplemented with 10% FCS. 5-7 days later, when the cells reached 60-70% confluency the fibroblasts were re-plated in 12-well culture plates at a density of  $10^5$  cells per well. After 3-5 hours allowing attachment of the cells, fibroblasts were transduced with shRNA<sub>mir</sub>-expressing lentivirus vectors at 10-30 m. o .i. 3 days later the culture medium was removed and the cells were lysed by adding 500  $\mu$ l Trizol reagent (Invitrogen) per well. Total RNA samples were purified from the lysates by following the manufacturer's protocols supplied with the Trizol reagent.

First-strand cDNA samples were generated from 0.5  $\mu$ g total RNA by the High Capacity cDNA Reverse Transcription Kit (Applied Biosystems) according to the manufacturer's instructions. SYBR-Green real time PCR reactions were performed on an MxPro 3000 platform (Stratagene), using SYBR Green PCR Master Mix (Applied Biosystems). Real time PCR data was analyzed by the Relative Expression Software Tool (REST) (54).



## Statistics

In the gene expression profiling experiment, group means were compared by Student's t-test. In other real time PCR experiments statistical analysis was done by the Pair Wise Fixed Reallocation Randomization Test implemented in REST software (54). Electrophysiological data was statistically analyzed by one-way ANOVA with Bonferroni's post-hoc test where applicable, by SPSS 13.0 for Windows software. Significance level was set as  $P < 0.05$  in all experiments.

## Results

### Expression pattern of $K^+$ -channel genes in the human heart

We designed PCR primer pairs for 31 ion channel genes. The well-known cardiac ion channels were selected at the first place, of which function in the heart has already been described. In addition, putative cardiac ion channel genes were also included in the study. The complete list of genes studied and the corresponding currents are shown in Table 3.

**Table 3.** List of the studied ion channel subunit genes. The currents to which the ion channel subunits presumably contribute in the human heart are presented in the 3<sup>rd</sup> and 6<sup>th</sup> columns.

Gene symbol	Alias	Function	Gene symbol	Alias	Function
Voltage gated $K^+$ channel subunits			Inward rectifier $K^+$ channel subunits		
<i>KCNA2</i>	Kv1.2	$I_{Kur}$	<i>KCNJ2</i>	Kir2.1	$I_{K1}$
<i>KCNA4</i>	Kv1.4	$I_{to}$	<i>KCNJ12</i>	Kir2.2	$I_{K1}$
<i>KCNA5</i>	Kv1.5	$I_{Kur}$	<i>KCNJ4</i>	Kir2.3	$I_{K1}$
<i>KCNA7</i>	Kv1.7	$I_{to}$	<i>KCNJ14</i>	Kir2.4	$I_{K1}$
<i>KCNB1</i>	Kv2.1	$I_{Kur}$	<i>KCNJ5</i>	Kir3.4	$I_{K-Ach}$
<i>KCNC1</i>	Kv3.1	$I_{Kur}$	<i>KCNJ8</i>	Kir6.1	$I_{K-ATP}$
<i>KCNC3</i>	Kv3.3	$I_{to}$	<i>KCNJ11</i>	Kir6.2	$I_{K-ATP}$
<i>KCNC4</i>	Kv3.4	$I_{to}$	Auxiliary $K^+$ channel subunits		
<i>KCND1</i>	Kv4.1	$I_{to}$	<i>KCNAB1</i>	Kv $\beta$ 1	$I_{Kur}$
<i>KCND3</i>	Kv4.3	$I_{to}$	<i>KCNAB2</i>	Kv $\beta$ 2	$I_{Kur}$
<i>KCNF1</i>	Kv5.1	silent	<i>KCNE1</i>	minK	$I_{Ks}$
<i>KCNS3</i>	Kv9.3	silent	<i>KCNE2</i>	MIRP1	$I_{Kr}$
<i>KCNH2</i>	hERG	$I_{Kr}$	<i>KCNE3</i>	MIRP2	$I_{Kr}$
<i>KCNQ1</i>	KvLQT1	$I_{Ks}$	<i>KCNIP2</i>	KChIP2	$I_{to}$
Two pore domain $K^+$ channel subunit			<i>KCNIP3</i>	CSEN	
<i>KCNK1</i>	TWIK1	$I_{K1}$	<i>ABCC8</i>	SUR1	$I_{K-ATP}$
			<i>ABCC9</i>	SUR2	$I_{K-ATP}$

### ***The $I_{to}$ -related $K^+$ channel subunits***

We studied the mRNA levels of six putative  $I_{to}$ -related voltage gated  $K^+$  channel subunits in the human left ventricle and left atrium. The comparative expression levels of the corresponding genes are as follows; ventricle:  $Kv1.7 > Kv4.3 > Kv3.4 >^* Kv1.4 >^* Kv4.1 >^* Kv3.3$ ; atrium:  $Kv1.7 > Kv4.3 > Kv3.4 > Kv4.1 > Kv1.4 >^* Kv3.3$  (Figure 14 A). The significant differences are labeled with an \* (here and in the rest of the 'Expression pattern of  $K^+$ -channel genes in the human heart' section). The  $Kv3.3$  and  $Kv4.1$  transcripts are at least ten times more abundant in the atrium as compared to the ventricle, while expression levels of  $Kv1.4$ ,  $Kv1.7$ ,  $Kv3.4$  and  $Kv4.3$  are similar in the two regions of the heart. Surprisingly, the expression level of  $Kv1.7$  and  $Kv3.4$  were high and fell into the same range as that of  $Kv4.3$  both in the ventricle and the atrium (48).

### ***The $I_{Kur}$ -related channel subunits***

Four  $K^+$  channel subunits have been identified thus far that produce currents in heterologous expression systems similar to the human  $I_{Kur}$ :  $Kv1.2$ ,  $Kv1.5$ ,  $Kv2.1$ ,  $Kv3.1$  (44). We found that the expression levels of these genes is  $Kv1.5 >^* Kv2.1 >^* Kv1.2 > Kv3.1$  in the atrium and  $Kv2.1 > Kv1.5 >^* Kv1.2 > Kv3.1$  in the ventricle (Figure 14 B).  $Kv1.5$  transcripts are approximately 30-fold more abundant in the atrium than in the ventricle. We found that  $Kv3.1$  was 5-fold more abundant in the atrium than in the ventricle, while there was no significant difference between the expression levels of  $Kv1.2$  and  $Kv2.1$  in the two regions of the heart (48).

### ***The $I_{Kr}$ - and $I_{Ks}$ -related subunits***

$I_{Kr}$  and  $I_{Ks}$  are the rapidly and slowly activating components of  $I_K$ . hERG subunits form those channels that are responsible for  $I_{Kr}$ , while  $I_{Ks}$  channels built up by  $KvLQT1$  subunits (13). It has turned out by comparing abundances of the pore-forming subunits of the two  $I_K$  components that hERG mRNA was significantly more abundant ( $P < 0.05$ ) than  $KvLQT1$  transcripts were in the ventricle, while the two genes were expressed at approximately the same level in the atrium. Both hERG and  $KvLQT1$  are expressed at a higher level than their possible interacting auxiliary subunits, both in the ventricle and atrium (Figure 14 C) (48).

### ***Modulatory 'silent' subunits of the $K^+$ channels***

We measured the expression level of two so-called 'silent' voltage gated  $K^+$  channel subunits:  $Kv5.1$  and  $Kv9.3$ . The  $Kv9.3$  message appears to be more abundant than that of  $Kv5.1$  in both the ventricle (is approximately 100 times more abundant) and in the atrium (is almost 10

times more abundant) (Figure 14 B). Both silent subunits are expressed at a significantly higher ( $P < 0.05$ ) level in the atrium compared to the ventricle. In addition, in the atrium Kv9.3 expression level is slightly higher ( $P < 0.05$ ) than that of its interacting partner Kv2.1 (48).

#### ***Auxiliary subunits of the voltage gated $K^+$ channels***

Kv $\beta$  subunits are cytosolic proteins and have been shown to co-assemble with members of the Kv1 subfamily (24). We designed primer pairs to amplify the cDNAs that correspond to the Kv $\beta$ 1- and the Kv $\beta$ 2-coding mRNAs. One primer pair recognizes all three known variants of Kv $\beta$ 1 mRNA and the other amplifies both of the two known Kv $\beta$ 2 variants. We detected both Kv $\beta$ -coding mRNAs in both of the left ventricles and atriums. Kv $\beta$ 1 was more abundant ( $P < 0.05$ ) than Kv $\beta$ 2 in the atrium, while there was no significant difference between the expression levels of the two genes in the ventricle (Figure 14 D). Furthermore, both Kv $\beta$  subunits seem to be upregulated in the atrium as compared to the ventricle ( $P < 0.05$ ) (48).

*KCNE* gene family consist of genes that encode membrane proteins (termed mink-related peptides; MiRPs) with one transmembrane domain interacting with Kv, KCNQ and ERG channels in heterologous expression systems (41). Until today, five members of the *KCNE* gene family have been described (38). We analyzed the expression level of three members of the *KCNE* gene family and established the following expression pattern in the atrium: KCNE1  $>^*$  KCNE3  $>^*$  KCNE2 (Figure 14 C) and confirmed results of Lundquist et al. (38). However, in contrast to the data published by Lundquist et al. (38) we did not detect significant differences in the abundances of the above transcripts in the ventricle (48).

#### ***The $I_{K1}$ - related inward rectifiers***

We analyzed the four known Kir2 subunits contributing to  $I_{K1}$  and measured similar expression patterns both in the ventricle (Kir2.3  $>^*$  Kir2.2  $>$  Kir2.4  $>$  Kir2.1) and atrium (Kir2.3  $>$  Kir2.2  $>^*$  Kir2.4  $>^*$  Kir2.1; Figure 14 E). With the exception of Kir2.2, which is almost 8-fold more abundant in the atrium than in the ventricle, all genes show the same expression levels in the two heart regions (48).

TWIK1 is a representative member of the so-called two-pore-domain  $K^+$  channel family and is thought to play a role in the formation of  $I_{K1}$ . It has turned out that abundance of the TWIK1-coding transcript is significantly higher (approximately 5-fold;  $P < 0.05$ ) in the atrium than in the ventricle. Furthermore, comparing the expression level of TWIK1 to that of the other subunits contributing to  $I_{K1}$  we learnt that the TWIK1-coding mRNA is most abundant in the atrium and the second most abundant in the ventricle (Figure 14 E) (48).

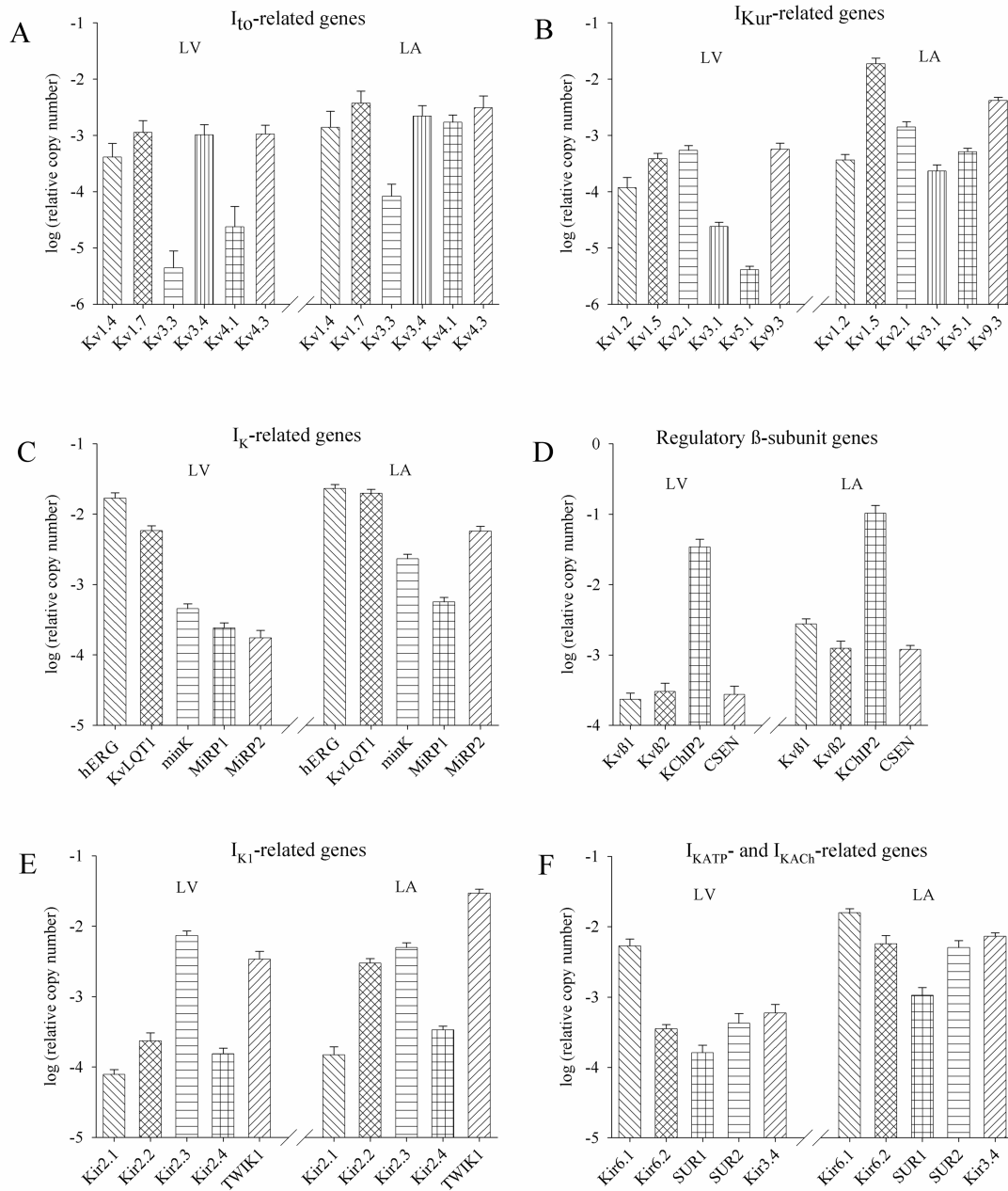


**Figure 14.** Relative expression level of the different ion channel subunit coding genes in the human heart as determined by real-time quantitative RT-PCR. The mRNA levels were quantified in tissue samples collected from the left ventricle (LV) and left atrium (LA). Data were normalized to the expression level of cytoplasmic  $\beta$ -actin and is presented as mean  $\pm$  SEM.

#### *The $I_{K-ATP}$ channel subunits*

We measured the expression level of two pore-forming subunits of  $I_{K-ATP}$  channels, Kir6.1 and Kir6.2. In  $I_{K-ATP}$  channels the Kir6.1 and the Kir6.2 subunits are associated with sulfonylurea

receptor subunits (SUR) depending on the tissue type. There are four human SUR isoforms: SUR1 and three splicing variants of SUR2 (SUR2A, SUR2B and SUR2A-delta-14). We designed one primer pair for SUR1 and another one that recognizes all of the three variants of SUR2. The expression pattern of the genes mentioned above is very similar in the two studied regions of the human heart: Kir6.1 is significantly the most abundant ( $P < 0.05$ ), Kir6.2 and SUR2 are less abundant and expressed at the same level compared to each other ( $P < 0.05$ ), while SUR1 shows the lowest ( $P < 0.05$ ) expression level (Figure 14 F). However, each of the four genes is expressed at a significantly higher level ( $P < 0.05$ ) in the atrium as compared to the ventricle (48).

### **Herpes-virus mediated gene transfer into cardiomyocytes**

Non-viral gene delivery methods perform well in most of the immortalized cell lines, however, they have limited efficiency in primary cells like post-mitotic cardiomyocytes. We explored the applicability of the *Pseudorabies virus* as a gene delivery vector in isolated adult cardiomyocytes (57). We constructed triple-attenuated viruses that carry either the Cameleon or the Troponin fluorescent marker genes. Deletions were generated in the *RR1*, *RR2* and *EP0* genes of the wild-type Kaplan strain of PRV (Figure 15 A) in two subsequent steps, resulting in the  $\Delta RR1$ , *RR2*, *EP0* genotype virus. As a third step of the vector construction, reporter gene cassettes were inserted into the inverted repeat region of the virus genome (Figure 15 A). Either the Cameleon or the Troponin  $Ca^{2+}$ -sensor reporter genes were used, resulting in the  $\Delta RR1$ , *RR2*, *EP0*, +*Cam* or in the  $\Delta RR1$ , *RR2*, *EP0*, +*Tropo* genotypes, respectively. Virus vectors of both aforementioned genotypes were used to infect isolated canine ventricular cardiomyocytes. The efficacy of the infections was high in both cases, reaching a virtual 100% efficiency, according to visual observations made by epifluorescent microscopy (Figure 15 B). There was no detectable increase in cell mortality in the virus infected group of cells compared to uninfected control cells (57). Moreover, the Troponin reporter gene, delivered by the PRV vector into canine cardiomyocytes, as assessed by FRET-analysis in contracting cardiomyocytes, has been shown to be functional (Figure 15 C) (57).

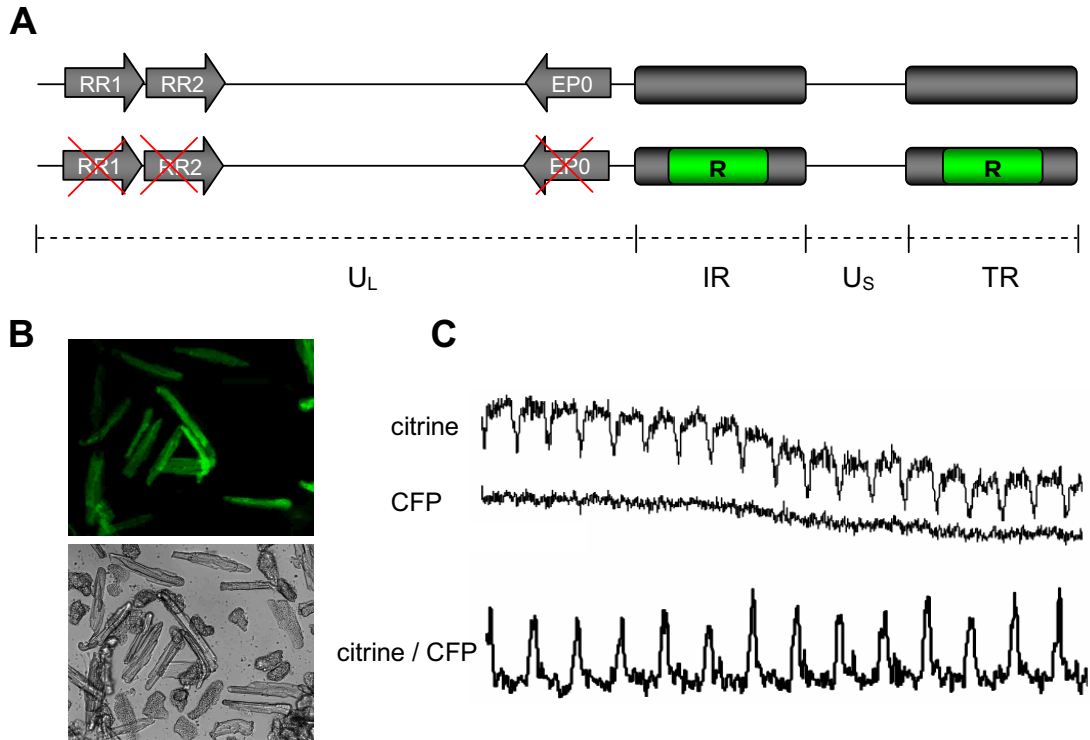


**Figure 15.** PRV is a potent gene delivery vector in isolated cardiomyocytes. **A:** Schematic representation of the genomic organization of the wild type Kaplan strain (upper bar) and that of the triple-attenuated vector strain (lower bar) of PRV. The triple-attenuated vector strain carries deletions in RR1, RR2 and EP0 genes and two copies of the Cameleon or Troponeon reporter genes (R). The scale bar in the bottom denote the four major genomic regions (UL: long unique, US: short unique, IR: internal repeat, TR: terminal repeat) of PRV. **B:** Photomicrographs show isolated canine ventricular cardiomyocytes 48 hours after infection by the  $\Delta RR1$ ,  $RR2$ ,  $EP0$ , +*Cam* PRV vector carrying the Cameleon reporter gene. **C:** Fluorescence emission traces recorded from contracting cardiomyocytes that were previously transfected by the  $\Delta RR1$ ,  $RR2$ ,  $RP0$ , +*Tropo* PRV vector expressing the Troponeon reporter gene. The recurrent peaks of the calculated citrine / CFP emission ratio indicate  $Ca^{2+}$  content increase in the cytoplasm during contractions. Fluorescence emission traces were taken from reference (57).

### Role of the MiRP2 regulatory subunit in $I_{to}$ channels

#### *Validating MiRP2 mRNA knock-down in canine atrial fibroblasts*

By gene expression profiling of ion channel genes in the human myocardium, among other interesting results we found that MiRP2 is abundantly expressed in both studied regions, particularly in the left atrium of the human heart. To assess possible role of MiRP2 in atrial cardiomyocytes, we created shRNAmir-expressing lentivirus vectors by which we aimed to generate functional MiRP2 knock-out cardiomyocytes by inducing RNAi targeted to the MiRP2 mRNA.

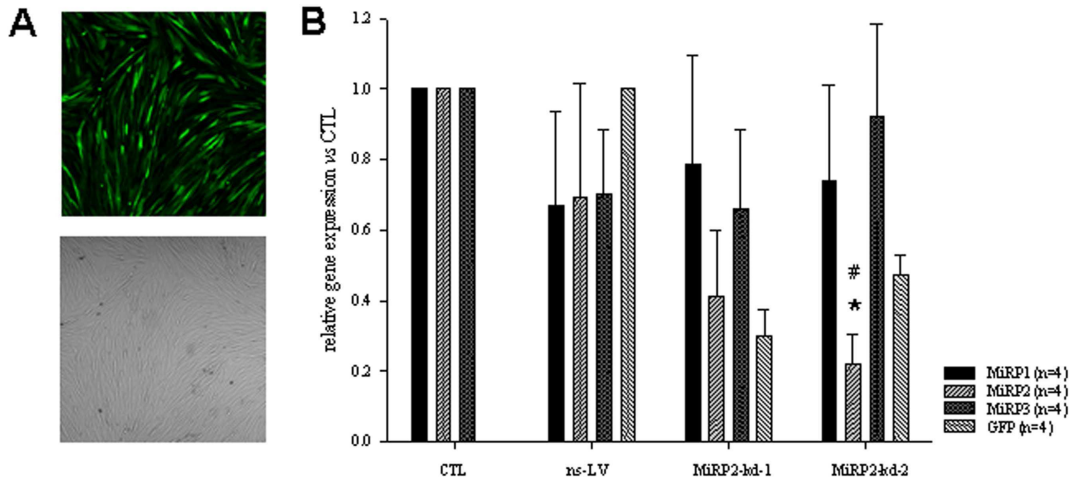


**Figure 16. A:** Photomicrograph examples show canine atrial fibroblasts infected by lentivirus vector at 10 m. o. i. **B:** Real time PCR results show efficient knock-down of the targeted MiRP2 mRNA in canine atrial fibroblasts. CTL: uninfected control, ns-LV: non-silencing lentivirus vector, MiRP-kd-1 and 2: lentivirus vectors expressing MiRP2-specific shRNAmirs. MiRP gene expression levels were normalized to CTL. To control virus load, gene expression level of the GFP was quantified and compared to that of the ns-LV group. Data is presented as mean  $\pm$  standard error of measurement, # shows significant difference vs CTL ( $P < 0.05$ ) and \* shows significant difference vs ns-LV ( $P < 0.05$ ).

To validate knock-down efficiency of the MiRP2 mRNA we used primary cultures of canine atrial fibroblasts as a model system. Real time PCR results showed an 80% knock-down vs uninfected control group and about 40% knock-down efficiency vs control group infected by a non-silencing lentivirus vector by one of our MiRP2-targeting lentivirus vectors (MiRP2-kd-2, Figure 16). mRNAs of the other two members of the KCNE gene family investigated (MiRP1 and MiRP3) were not affected.

#### ***Effect of MiRP2 knock-down on macroscopic $I_{to}$ parameters***

To evaluate possible role of MiRP2 in  $I_{to}$  channels, we functionally knocked down MiRP2 in isolated canine atrial cardiomyocytes by using our pre-validated lentivirus vector targeting MiRP2 (MiRP2-kd-2, Figure 17).

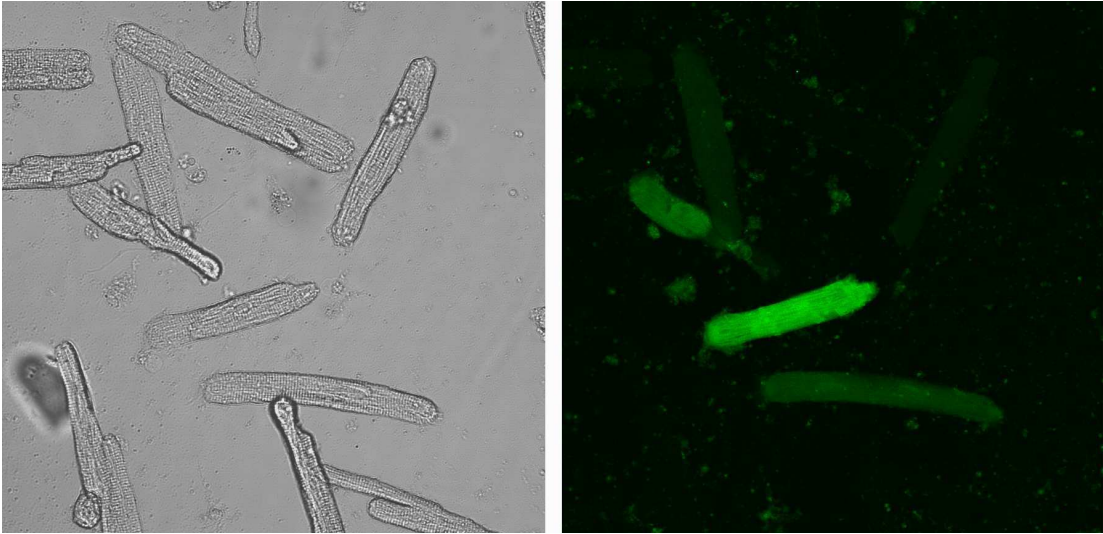


**Figure 17.** Photomicrograph examples show canine atrial cardiomyocytes infected by the MiRP2-targeting lentivirus vector. Images were taken 72 hours after infection.

$I_{to}$  was characterized by the whole-cell voltage clamp method in freshly isolated cells (Fresh), in cultured cells with no virus added (CTL group) and in cultured cells that were infected by either a control lentivirus vector expressing GFP only (empty LV), a control lentivirus vector expressing a non-silencing shRNAmir (ns LV) or the MiRP2-targeting lentivirus vector (MiRP2-kd-2) 72 hours after infection. The summary of our results is shown in Table 4.

**Table 4.** Effect of MiRP2 knock-down on macroscopic  $I_{to}$  parameters in canine atrial cardiomyocytes. Data is presented as mean  $\pm$  SEM. +, \$, # and \* represent significant difference vs Fresh, CTL, empty LV and ns LV, respectively.

	Current density		Activation		SS-act.		SS-inact.	
	(pA/pF, +50mV)	n	TtP (ms, +50mV)	n	$V_{0.5}$ (mV)	n	$V_{0.5}$ (mV)	n
Fresh	$7.5 \pm 1.1$	8	$4.8 \pm 0.5$	8	$9.0 \pm 1.1$	6	$-30.8 \pm 2.4$	8
CTL	$11.4 \pm 0.9$	12	$5.7 \pm 0.2$	12	$3.2 \pm 1.8$	7	$-25.4 \pm 1.2$	9
empty LV	$14.0 \pm 1.1$ <sup>+</sup>	9	$5.0 \pm 0.2$	8	$6.3 \pm 2.9$	4	$-29.3 \pm 1.7$	6
ns LV	$12.0 \pm 1.1$	6	$5.8 \pm 0.3$	6	$8.8 \pm 2.2$	6	$-25.6 \pm 1.9$	6
MiRP2-kd-2	$15.1 \pm 1.6$ <sup>+</sup>	7	$5.5 \pm 0.4$	5	$4.9 \pm 0.6$	4	$-20.9 \pm 0.7$ <sup>+</sup>	4
	$\tau$ fast (ms, +50mV)		$\tau$ slow (ms, +50mV)		$A_{fast}/(A_{fast}+A_{slow})$ (% , +50mV)			
Fresh	$5 \pm 0.7$		$24.5 \pm 5.8$		$51.8 \pm 4.2$			
CTL	$10.4 \pm 1.7$ <sup>+</sup>		$44.3 \pm 3.6$		$28.1 \pm 3.7$ <sup>+</sup>			
empty LV	$9.8 \pm 1.5$		$44.8 \pm 5.3$		$35.8 \pm 5.6$			
ns LV	$8.9 \pm 1.2$		$35.2 \pm 4.9$		$32.5 \pm 7.0$			
MiRP2-kd-2	$18.2 \pm 1.6$ <sup>+\$#*</sup>		$100.0 \pm 24.1$ <sup>+\$#*</sup>		$28.0 \pm 5.3$ <sup>+</sup>			



### Current-voltage relations

Current-voltage relations of  $I_{to}$  were elucidated by voltage steps from a holding potential at -50 mV to -40 to +50 mV. When measured at +50 mV,  $I_{to}$  densities were significantly increased in two of the virus-infected groups ( $14.0 \pm 1.1$ ,  $n=9$ , empty LV and  $15.1 \pm 1.6$ ,  $n=7$ , MiRP-kd-2) compared to Fresh ( $7.5 \pm 1.1$ ,  $n=8$ ) (Table 4), but MiRP2 knock-down had no significant effect compared to CTL or to the ns LV group (Figure 18).

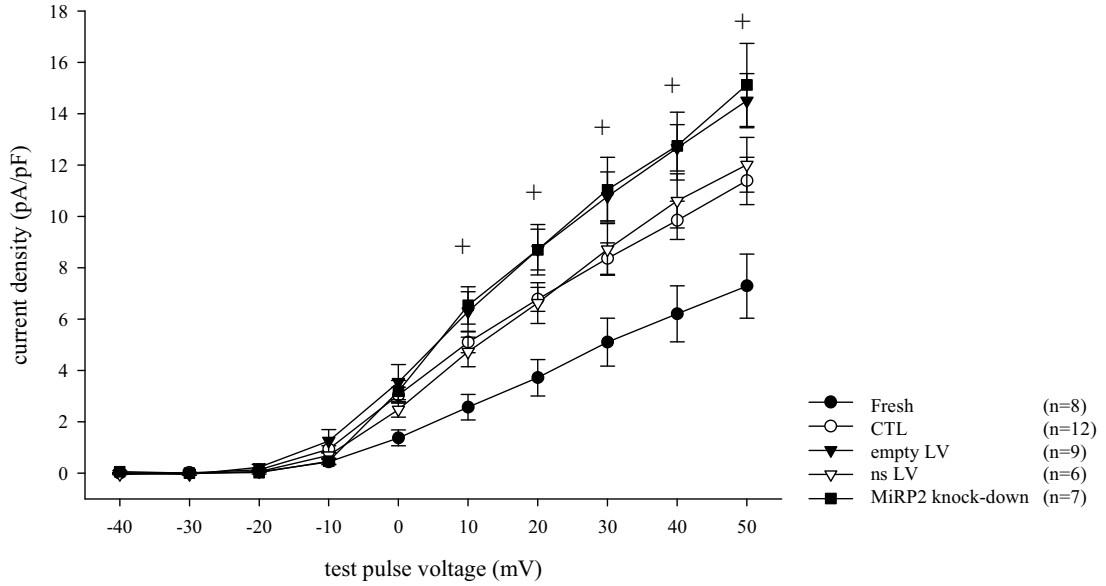


**Figure 18.** Current-voltage relations. Data is presented as mean  $\pm$  SEM. Statistics is shown for the MiRP2 knock-down group only. + represents  $P < 0.05$  vs Fresh.

### Voltage-dependence of activation and inactivation

The steady-state activation values were calculated from current-voltage relations. Reversal potentials were measured for each cell and were corrected by the liquid junction potential (-10 mV). Half-maximal activation voltage was not significantly different between the experimental groups (Table 4, Figure 19). Steady-state inactivation of  $I_{to}$  was evaluated by using a standard prepulse-test pulse voltage clamp protocol. The  $I_{to}$  amplitude was determined and plotted as a function of prepulse voltage. Half-maximal inactivation voltage in MiRP2 knock-down group was significantly less negative than in the Fresh group ( $-20.9 \pm 0.7$ ,  $n=4$  vs  $-30.8 \pm 2.4$ ,  $n=8$ ), but ANOVA did not detect significant differences between MiRP2-kd-2 and ns LV or empty LV groups (Table 4, Figure 19).

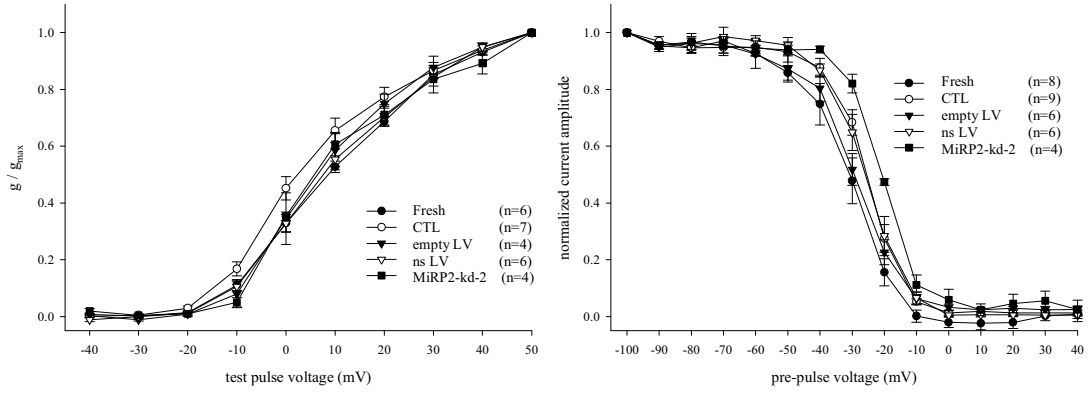


**Figure 19.** Steady-state gating of  $I_{t0}$ . Left panel: activation voltage dependence. Right panel: voltage dependence of inactivation.

#### *Time course of activation and inactivation*

We also analyzed the effect of MiRP2 knock-down on activation and inactivation kinetics of  $I_{t0}$ . Time course of activation was evaluated by measuring time to peak current (TtP). MiRP2 knock-down had no effect on activation kinetics (Table 4, Figure 20 A). Time course of inactivation was elucidated by fitting biexponential function ( $f(t) = A_{\text{slow}} e^{-t/\tau_{\text{slow}}} + A_{\text{fast}} e^{-t/\tau_{\text{fast}}}$ ) to individual current traces. Time constant of the fast component of inactivation ( $\tau_{\text{fast}}$ ) was significantly increased in the MiRP2 knock-down group ( $18.2 \pm 1.6$ ,  $n = 6$ ) compared to the ns LV group ( $8.9 \pm 1.2$ ,  $n = 6$ ) at +50 mV test pulse (Table 4, Figure 20 B). Similarly, time constant of the slow inactivation component ( $\tau_{\text{slow}}$ ) increased significantly in MiRP2 knock-down group ( $100.0 \pm 24.1$ ,  $n = 6$ ) vs ns LV group ( $35.2 \pm 4.9$ ,  $n = 6$ ) (Table 4, Figure 20 D). Relative contribution of the fast inactivation component to total  $I_{t0}$  inactivation was analyzed by comparing the amplitude of the fast inactivation component ( $A_{\text{fast}}$ ) to the total amplitude ( $A_{\text{fast}} + A_{\text{slow}}$ ). The fast component contributes significantly less to total  $I_{t0}$  inactivation in the CTL group ( $28.1 \pm 3.7$ ,  $n=11$ ) vs Fresh ( $51.8 \pm 4.2$ ,  $n = 11$ ), but MiRP2 knock-down had no significant effect compared to CTL, empty LV or ns LV groups (Table 4, Figure 20 C).

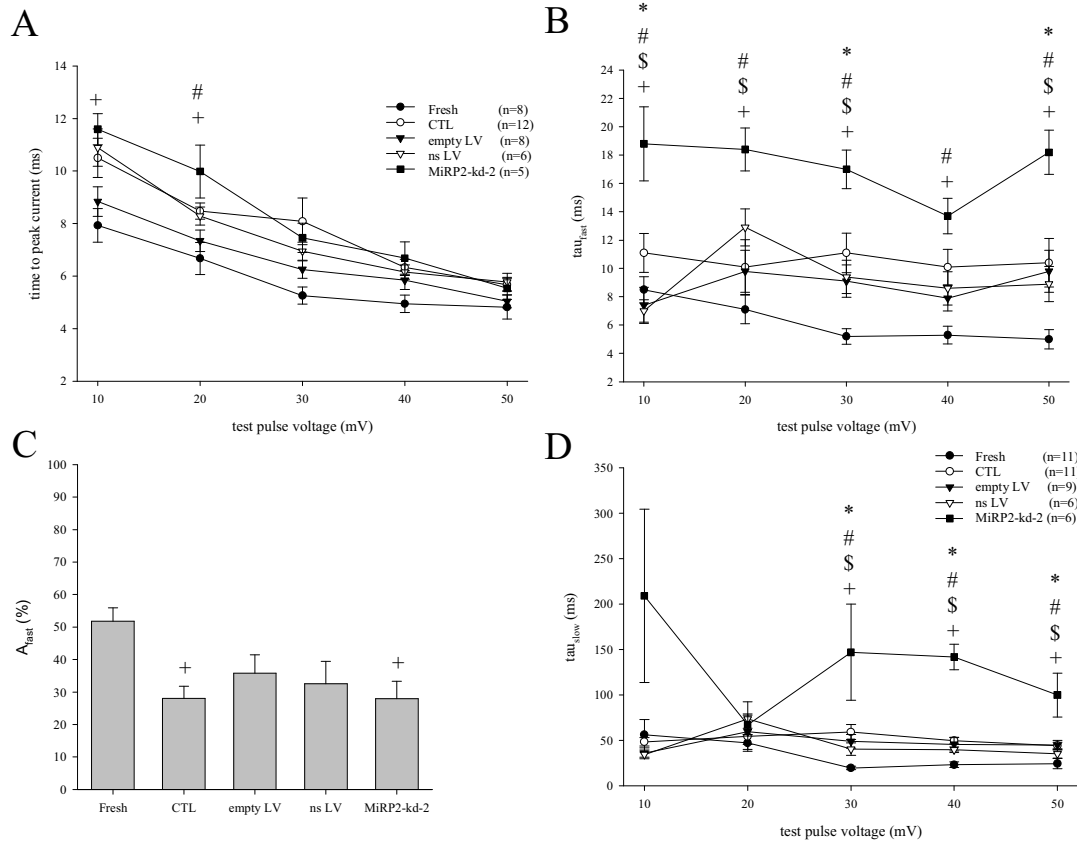


**Figure 20. A:** Time to peak (TtP). **B:** Time constant of the fast inactivation component ( $\tau_{fast}$ ). **C:** Relative contribution of the fast inactivation component ( $A_{fast}$ ) to inactivation. **D:** Time constant of the slow inactivation component ( $\tau_{slow}$ ). Data is presented as mean  $\pm$  SEM. +, \$, # and \* represent significant difference vs Fresh, CTL, empty LV and ns LV, respectively. Figure legend for panel B and D is shown in panel D.

## Discussion

### Expression pattern of $K^+$ -channel genes in the human heart

In 2006 we reported among the first ones the gene expression level of a comprehensive set of ion channel genes in the undiseased human myocardium (48). We aimed to confirm and analyze the expression and relative abundance of mRNAs of the well-known ion channel genes, which may help us to extrapolate findings obtained in model organisms to the human heart. In addition, based on the notion that many more ion channel genes exist than ion currents we know, we extended the focus of this study on novel cardiac ion channel gene candidates. We carefully collected data available in the literature and selected new genes to include in the study if one of the two following criteria was met: i) the expression of the cardiac ion channel gene candidate has been shown in cardiac tissues of model organisms but not in the human heart, ii) an interaction between the cardiac ion channel candidate and a

well-known cardiac ion channel has been shown by co-expression studies or by means of biochemical techniques detecting protein-protein interactions. We reported the high expression level of novel cardiac ion channel gene candidates, of which possible role in the heart has not been considered previously. Therefore, our gene expression profiling data may serve as a basis for the design of studies aiming to reveal new ion channel gene functions in the human heart. We discuss our most important findings below.

### ***The $I_{to}$ -related $K^+$ channel subunits***

$I_{to}$  is generally considered to have two components, one based on Kv4.2/Kv4.3 alpha subunits showing rapid recovery from inactivation, and one that recovers slowly from inactivation and is based on Kv1.4 (53). We analyzed the expression level of six putative  $I_{to}$ -related  $K^+$  channel genes: Kv1.4 (55), Kv1.7 (32), Kv3.3 (79), Kv3.4 (68), Kv4.1 (51) and Kv4.3 (69). These ion channels produce currents with fast activation and rapid inactivation kinetics in heterologous expression systems, therefore they are possible candidates for physiologically important  $I_{to}$  subunits. Nevertheless, the literature is bountiful regarding their expression in the human heart. Kv1.4 has not yet been detected in human heart by Western blot analysis (78). Furthermore, the same study showed no effect of antisense oligonucleotides targeted against the Kv1.4 transcripts on human atrial  $I_{to}$  (78). In contrast, in more recent studies it has been shown that Kv1.4 is expressed in the human atrium (6) and ventricle (74). Expression of Kv1.7 has also been described in the human heart (5), but its function has not yet been elucidated. There is no data in the literature on the expression of the Kv3.3 and Kv3.4 genes in the human heart. Kv3.3 and Kv3.4 transcripts have not been detected in rat heart (47), however, the presence of Kv3.4 protein has been shown by immunohistochemical studies and western blots both in canine Purkinje fibers and canine ventricular muscle (26). The Kv4.1 and Kv4.3 coding mRNAs have also been shown to be expressed in human heart (30). We detected all of the six putative  $I_{to}$  channel coding mRNAs in the human heart (48), including Kv3.3 and Kv3.4, which have not been described in human cardiac tissues previously. Furthermore, we have shown that expression levels of Kv1.7 and Kv3.4 are high and fell into the same range as that of Kv4.3 both in the ventricle and in the atrium (48).

In heterologous expression systems the current produced by Kv1.7 or Kv4.3 is insensitive for TEA (32), while Kv3.4 current is blocked by TEA (68). In the dog, ventricular  $I_{to}$  is not sensitive for TEA, while in Purkinje fibers a prominent block of  $I_{to}$  by TEA was reported (27). Kv3.4 protein is more abundant in canine Purkinje fibers than in ventricular muscle and Kv3.4 was suggested as a candidate responsible for the larger TEA-sensitive  $I_{to}$  component in Purkinje fibers (26). On the other hand, we found relatively high expression level of Kv3.4 in

the ventricle where  $I_{to}$  is not blocked by TEA. It thus remains to be determined whether Kv3.4 plays a role in the formation of ventricular  $I_{to}$  and whether the TEA sensitivity of Purkinje cell  $I_{to}$  is due to the presence of Kv3.4 or possibly due to associated accessory subunits.

### ***The $I_{Kur}$ -related channel subunits***

$I_{Kur}$  is driven by Kv1.5 (20) and is a substantial current in atrial cells, but appears to be absent in the ventricle. Accordingly we found that Kv1.5 transcripts are much more abundant in the atrium than in the ventricle (48). Kv2.1 generates currents sharing characteristic features with Kv1.5 and  $I_{Kur}$  in heterologous expression systems (44). Interestingly, we found significant expression levels of the Kv1.5- and the Kv2.1-coding genes in the human ventricular samples (48). This observation suggests a possible functional role of the subunits in the human ventricle. Since  $I_{Kur}$  has not been observed in the human ventricle, it is frequently considered as the possible target of atrium-specific antiarrhythmic drugs (65, 76). Atrium-specific blocking of  $I_{Kur}$  channels may help in chemical treatment of atrial fibrillation avoiding elongated action potential durations in the ventricles, which would increase the risk of ventricular arrhythmias. However, the presence of  $I_{Kur}$ -related ion channel subunits in the human ventricle indicates a possible limitation of the applicability of  $I_{Kur}$  blockers in treatment of atrial fibrillation without imposing proarrhythmic risk on the ventricle.

### ***Modulatory ‘silent’ alpha-subunits of $K^+$ channels***

The members of Kv5 – Kv11 subfamilies are electrically silent in homotetrameric configuration, however, they show all structural characteristics of voltage gated  $K^+$  channels (49). They co-assemble with other voltage gated  $K^+$  channel subunits and modulate the function of the heteromeric ion channel complex. Both silent subunits studied here (Kv5.1 and Kv9.3) are thought to alter the kinetic parameters of currents produced by Kv2.1 (34, 52, 63). Kv2.1 and Kv9.3 have been shown to co-assemble in heteromeric channels in a 3 : 1 stoichiometry (33). Evidences showing interaction between the two studied silent subunits and Kv2.1 indicate that these regulatory silent subunits may be involved in the formation of the  $I_{Kur}$  channels. According to our knowledge we reported the expression of Kv5.1 and Kv9.3 modulatory alpha-subunits in the human heart. Our data shows a higher expression level of both Kv5.1 and the Kv9.3 in the atrium compared to the ventricle (48), which finding is consistent with the known uneven distribution of  $I_{Kur}$  densities in these two regions of the heart. Confirming the possible function of Kv5.1 and Kv9.3 in the heart may help to refine our present view on the nature and number of possible interactions between ion channel subunits.

### ***Auxiliary subunits of the K<sup>+</sup> channels***

We measured the expression level of three members of the *KCNE* gene family. There is strong evidence showing that I<sub>Kr</sub> is produced by hERG/MiRP1 (*KCNE2*)/mink (*KCNE1*) channels (2, 42) and I<sub>Ks</sub> is generated by KvLQT1/minK (*KCNE1*) channels (66). We, among the very first ones, reported relatively high expression of a recently described member of the *KCNE* gene family MiRP2 (*KCNE3*) in the human heart (48). This abundant MiRP2 expression encouraged us to perform further experiments to clarify MiRP2 function by the means of RNAi technology. Our findings and the possible role of MiRP2 in the myocardium is discussed later in the 'Role of MiRP2 regulatory subunit in Ito channels' section.

### **Herpes-virus mediated gene transfer into cardiomyocytes**

*Pseudorabies virus* (PRV) is best known for its ability to spread through synapses between nerve cells in the central nervous system. PRV has been used for delivering genetic material to neurons and for labeling neuronal circuits (56). According to our knowledge, PRV has not been used as a gene delivery tool in cardiomyocytes. PRV is able to infect and maintain life-long infections in post-mitotic neurons and our pilot experiments showed that under experimental conditions PRV infects cardiomyocytes as well. However, previous studies showed that the wild-type virus has cytopathic effects, which hampers its applicability as a gene transfer vector of experimental or therapeutic use (8). In general, a potent viral gene transfer vector has no or reasonably low toxic and other side-effects, allows long-term transgene expression and retains its capability to replicate under certain conditions. We developed a multiply attenuated PRV strain by the step-wise introduction of mutations into the wild-type PRV genome to meet the aforementioned requirements. Specific mutations were selected based on previously published data available in the literature.

The large (RR1) and small (RR2) subunits of ribonucleotide reductase enzyme (RR) is encoded by two separate ORFs in the PRV genome (Figure 10 and Figure 15 A) (56). RR is involved in nucleotide metabolism, it catalyzes the reduction of ribonucleotides into deoxyribonucleotides, the substrates for DNA synthesis. In a previous study it has been shown that PRV strains carrying mutation in RR1 are severely attenuated in post-mitotic or growth arrested cells, but are able to replicate in dividing cultured cells (16). We deleted a 1.8 Kb portion of the PRV genome affecting both the RR1 and RR2 ORFs, thereby generating an RR deficient virus. The RR deficient virus retains its replication capacity in cultured cells where deoxyribonucleotides produced by cellular enzymes are available, while its virulence and therefore its cytotoxicity is much lower in post-mitotic cells, such as cardiomyocytes.

The *EP0* gene of PRV is transcribed with early kinetics and encodes a transcriptional transactivator protein, regulating gene expression from several viral promoters (Figure 10 and Figure 15 A) (56). *EP0* is dispensable for viral growth and therefore *EP0* deficient virus vectors can be multiplied in cultured cells, however, viral titers and plaque sizes are reduced compared to the wild-type virus. On the other hand, *EP0* negative PRV mutants are attenuated *in vivo* (8). These properties of *EP0* make the  $\Delta EP0$  mutation an ideal selection for the development of a low-virulence gene transfer vector.

During viral gene transfer, in addition to avoiding cytotoxic effects, the relatively long-term transgene expression should be preferably maintained. While many PRV genes, such as genes encoding viral structural proteins, are only expressed during the lytic infection, latency associated transcripts (LATs) – although in different sizes – can be detected during the lytic cycle and latency as well. Therefore, LAT promoters and downstream regions represent transcriptionally active landmarks of the PRV genome. As an insertion site of transgenes we selected a downstream area of a putative LAT promoter (ASP, Figure 10) (10), which is located in the inverted repeats and hence it is present in two copies in the PRV genome. The ASP region, therefore, ensures abundant transgene expression levels due to the double copy number of transgenes regardless of the virus life cycle stage.

With the  $\Delta RRI1$ , *RR2*, *EP0* PRV strain we were able to introduce transgenes into adult isolated cardiomyocytes. The transduced cells showed no obvious cytopathic effects. In addition, we have shown that the delivered activity markers remained fully functional. Our modified PRV strain represents a viable option for gene transfer vectors in cardiovascular research.

### **Role of MiRP2 regulatory subunit in $I_{to}$ channels**

MiRP2 has been first described as the interacting partner of KvLQT1 in a heterologous expression system. MiRP2/KCNQ1 channels have been shown to form a constitutively open ion channel and their role in intestinal chloride secretion has been suggested (67). Accordingly, ectopic expression of MiRP2 in guinea pig ventricles abbreviated QT interval, possibly due to MiRP2-KCNQ1 interactions which led to an increased  $I_{Ks}$  density (40). In skeletal muscle MiRP2 has been shown to interact with Kv3.4 and a MiRP2 mutation has been shown to co-associate with periodic paralysis (1). More recently, an interaction between MiRP2 and a typical  $I_{to}$  channel Kv4.3 has been shown in a co-expression study (37). Moreover, a loss-of-function MiRP2 mutation associated with Brugada syndrome affecting Kv4.3 current density and kinetics has been identified (17). MiRP2 seems to decrease densities and slow inactivation kinetics of Kv4.3 currents, without affecting steady-state

gating parameters and the overall effect is a decreased  $I_{Kv4.3}$  magnitude (17). There are multiple evidences showing that the main regulatory subunit modulating Kv4.3 channel function in the heart is KChIP2 (reviewed in 53). Interestingly, when Kv4.3 was expressed in the presence of both KChIP2 and MiRP2 in a triple co-expression system, MiRP2 did not affect current densities, but decreased time constants of both activation and inactivation and shifted half-maximal inactivation voltage to more negative potentials (58). Therefore it seems that the modulatory function of MiRP2 on Kv4.3 current depends on the presence of other auxiliary subunits, such as KChIP2. MiRP2 decreases current magnitude when Kv4.3 is expressed alone, while MiRP2 has no effect on current density but accelerates activation and inactivation and shifts steady-state inactivation curves of Kv4.3/KChIP2 channels to more negative potentials.

Since KChIP2 has been suggested to be an obligatory subunit of native  $I_{to}$  (35), it is reasonable to assume that both KChIP2 and MiRP2 play a role in the formation of native  $I_{to}$  channels. Our findings strongly support the latter hypothesis. With a lentivirus-based vector system we delivered artificial microRNAs into canine atrial cardiomyocytes to knock-down MiRP2 expression. MiRP2 knock-down had no effect on current density, but significantly slowed down inactivation kinetics of  $I_{to}$ , which is consistent with the published data on Kv4.3/KChIP2/MiRP2 channels. In our experiments, MiRP2 did not affect the steady-state inactivation parameters, however, with the existing number of cases ( $n=4$ ) in that experiment we cannot draw reliable conclusions in this regard.

The strength of our experimental system is that we were able to show data on the regulatory role of MiRP2 in  $I_{to}$  channels of cardiomyocytes *in situ* by the first time and our data is consistent with predictions made in *in vitro* experimental systems. Among the weaknesses we should mention that there seems to be a remodeling process taking place in cultured cardiomyocytes, which results in changes in cellular electrophysiology. Several currents that can be recorded in freshly isolated cells, such as  $I_{Ks}$  and  $I_{K1}$ , go nearly undetectable in cultured cells (data not shown). Kinetic and steady-state gating parameters of  $I_{to}$  are mainly unaffected during culture, however, current densities are significantly higher in cultured cells compared to freshly isolated ones and the contribution of the fast inactivation component to  $I_{to}$  inactivation is less prominent in cultured vs fresh cells. These latter differences strongly suggest remodeling in the expression level of one or more  $I_{to}$  channel subunits during culturing. The better understanding of the remodeling process in cultured cardiomyocytes would help us not only to better interpret the MiRP2 knock-down data, but also to better recognize the possible limitations and applicability of our experimental system in general.



## Summary

Ion channels are one of the key determinants of heart function and are of primary importance in the pathophysiology of heart rhythm disorders. Moreover, they show an extreme functional diversity as well. In this work we aimed to lay the fundamentals for new approaches to study the function of individual ion channel subunits.

We studied the gene expression level of a large selection of known and putative cardiac ion channel genes in the human heart. Our work – showing up a cross-section of an important part of the human cardiac transcriptome – provides a substantial insight into the molecular basis of ionic currents in the human heart muscle. As a functional genomics approach, our study raises many intriguing questions about the function of specific ion channel subunits and may serve as the foundation for forthcoming functional studies.

Despite the recent enormous advances in the field of the development of virus-based gene transfer methods it seems that the ultimate vector for cardiac gene delivery that fulfills the versatile needs of experimental work and also meets the special requirements of gene therapy has not been found yet. Here we report the development of a gene transfer vector based on the *Pseudorabies virus*. Our multiply attenuated virus vector efficiently transduces isolated adult cardiomyocytes and represents a viable alternative for the existing viral gene delivery methods in cardiovascular research.

We report among the first ones the expression of a novel auxiliary ion channel subunit MiRP2 in the human heart. Based on data obtained in co-expression studies, MiRP2 has been suggested to play a regulatory role in  $I_{to}$  channels. To assess the possible function of MiRP2 in heart muscle cells we combined viral gene transfer with the RNA interference technology. We show that MiRP2 accelerates the time course of inactivation of  $I_{to}$  channels in atrial cardiomyocytes.

Our experimental system will help us to unveil subunit-specific functions and multiple interactions that are anticipated among ion channel subunits and will help us to set ground for therapeutic strategies as we press forward in the field of gene therapy of cardiac arrhythmias.

## References

- 1) Abbott GW, Butler MH, Bendahhou S, Dalakas MC, Ptacek LJ, Goldstein SA. MiRP2 forms potassium channels in skeletal muscle with Kv3.4 and is associated with periodic paralysis. *Cell* 2001; 104(2):217-31.
- 2) Abbott GW, Sesti F, Splawski I, Buck ME, Lehmann MH, Timothy KW, Keating MT, Goldstein SA. MiRP1 forms IKr potassium channels with HERG and is associated with cardiac arrhythmia. *Cell* 1999; 97: 175–87.
- 3) Armstrong CM, Bezanilla F. Inactivation of the sodium channel. II. Gating current experiments. *J Gen Physiol.* 1977; 70(5): 567–90.
- 4) Balser JR. The cardiac sodium channel: gating function and molecular pharmacology. *J Mol Cell Cardiol.* 2001; 33(4): 599–613.
- 5) Bardien-Kruger S, Wulff H, Arieff Z, Brink P, Chandy KG, Corfield V. Characterisation of the human voltage-gated potassium channel gene, KCNA7, a candidate gene for inherited cardiac disorders, and its exclusion as cause of progressive familial heart block I (PFHBI). *Eur J Hum Genet.* 2002; 10(1): 36–43.
- 6) Bertaso F, Sharpe CC, Hendry BM, James AF. Expression of voltage-gated K<sup>+</sup> channels in human atrium. *Basic Res Cardiol.* 2002; 97(6): 424–33.
- 7) Beuckelmann DJ, Näbauer M, Erdmann E. Alterations of K<sup>+</sup> currents in isolated human ventricular myocytes from patients with terminal heart failure. *Circ Res.* 1993; 73(2): 379–85.
- 8) Boldogkoi Z, Braun A and Fodor I. Replication and virulence of early protein 0 and long latency transcript deficient mutants of the Aujeszky's disease (pseudorabies) virus. *Microbes Infect* 2000; 2(11):1321–1328.
- 9) Boldogkoi Z, Braun A, Antal J and Fodor I. A restriction cleavage and transfection system for introducing foreign DNA sequences into the genome of a herpesvirus. *Res Virol* 1998; 149(2):87–97.
- 10) Boldogkoi Z, Erdelyi F and Fodor I. A putative latency promoter/enhancer (P(LAT2)) region of pseudorabies virus contains a virulence determinant. *J Gen Virol* 2000; 81(2):415–420.
- 11) Bonci D, Cittadini A, Latronico MV, Borello U, Aycock JK, Drusco A, Innocenzi A, Follenzi A, Lavitrano M, Monti MG, Ross J Jr, Naldini L, Peschle C, Cossu G, Condorelli G. 'Advanced' generation lentiviruses as efficient vectors for cardiomyocyte gene transduction in vitro and in vivo. *Gene Ther* 2003; 10(8):630-6.
- 12) Chen Q, Kirsch GE, Zhang D, Brugada R, Brugada J, Brugada P, Potenza D, Moya A, Borggrefe M, Breithardt G, Ortiz-Lopez R, Wang Z, Antzelevitch C, O'Brien RE, Schulze-Bahr E, Keating MT, Towbin JA, Wang Q. Genetic basis and molecular mechanism for idiopathic ventricular fibrillation. *Nature.* 1998; 392(6673): 293–6.
- 13) Cheng JH, Kodama I. Two components of delayed rectifier K<sup>+</sup> current in heart: molecular basis, functional diversity, and contribution to repolarization. *Acta Pharmacol Sin.* 2004; 25(2): 137–45.
- 14) Chiang CE, Roden DM. The long QT syndromes: genetic basis and clinical implications. *J Am Coll Cardiol.* 2000; 36(1): 1–12.
- 15) Coetzee WA, Amarillo Y, Chiu J, Chow A, Lau D, McCormack T, Moreno H, Nadal MS, Ozaita A, Pountney D, Saganich M, Vega-Saenz de Miera E, Rudy B. Molecular diversity of K<sup>+</sup> channels. *Ann N Y Acad Sci.* 1999; 868: 233–85.
- 16) de Wind N, Berns A, Gielkens A, Kimman T. Ribonucleotide reductase-deficient mutants of pseudorabies virus are avirulent for pigs and induce partial protective immunity. *J Gen Virol* 1993;74 ( Pt 3):351-9.

- 17) Delpón E, Cordeiro JM, Núñez L, Thomsen PE, Guerchicoff A, Pollevick GD, Wu Y, Kanters JK, Larsen CT, Hofman-Bang J, Burashnikov E, Christiansen M, Antzelevitch C. Functional effects of KCNE3 mutation and its role in the development of Brugada syndrome. *Circ Arrhythm Electrophysiol* 2008; 1(3):209-18.
- 18) Doyle DA, Morais Cabral J, Pfuetzner RA, Kuo A, Gulbis JM, Cohen SL, Chait BT, MacKinnon R. The structure of the potassium channel: molecular basis of K<sup>+</sup> conduction and selectivity. *Science*. 1998; 280(5360): 69–77.
- 19) Ekstrand MI, Enquist LW, Pomeranz LE. The alpha-herpesviruses: molecular pathfinders in nervous system circuits. *Trends Mol Med* 2008;14(3):134-40.
- 20) Feng J, Wible B, Li GR, Wang Z, Nattel S. Antisense oligodeoxynucleotides directed against Kv1.5 mRNA specifically inhibit ultrarapid delayed rectifier K<sup>+</sup> current in cultured adult human atrial myocytes. *Circ Res* 1997; 80: 572–9.
- 21) Ferrier GR, Howlett SE. Cardiac excitation-contraction coupling: role of membrane potential in regulation of contraction. *Am J Physiol Heart Circ Physiol*. 2001; 280(5): H1928–44.
- 22) Gauthier ER, Madison SD, Michel RN. Rapid RNA isolation without the use of commercial kits: application to small tissue samples. *Pflugers Arch* 1997; 433: 664–8.
- 23) Goldstein SA. A structural vignette common to voltage sensors and conduction pores: canaliculi. *Neuron*. 1996; 16(4): 717–22.
- 24) Gulbis JM, Zhou M, Mann S, MacKinnon R. Structure of the cytoplasmic beta subunit-T1 assembly of voltage-dependent K<sup>+</sup> channels. *Science*. 2000; 289(5476): 123–7.
- 25) Hajjar RJ, del Monte F, Matsui T, Rosenzweig A. Prospects for gene therapy for heart failure. *Circ Res* 2000; 86(6):616-21.
- 26) Han W, Bao W, Wang Z, Nattel S. Comparison of ion-channel subunit expression in canine cardiac Purkinje fibers and ventricular muscle. *Circ Res*. 2002; 91: 790–7.
- 27) Han W, Wang Z, Nattel S. A comparison of transient outward currents in canine cardiac Purkinje cells and ventricular myocytes. *Am J Physiol Heart Circ Physiol*. 2000; 279: H466–74.
- 28) Hannon GJ. RNA interference. *Nature*. 2002; 418(6894):244-51.
- 29) Hoshi T, Zagotta WN, Aldrich RW. Two types of inactivation in Shaker K<sup>+</sup> channels: effects of alterations in the carboxy-terminal region. *Neuron*. 1991; 7(4): 547–56.
- 30) Isbrandt D, Leicher T, Waldschütz R, Zhu X, Luhmann U, Michel U, Sauter K, Pongs O. Gene structures and expression profiles of three human KCND (Kv4) potassium channels mediating A-type currents I(TO) and I(SA). *Genomics* 2000; 64: 144–54.
- 31) Isomoto S, Kondo C, Kurachi Y. Inwardly rectifying potassium channels: their molecular heterogeneity and function. *Jpn J Physiol*. 1997; 47(1): 11–39.
- 32) Kalman K, Nguyen A, Tseng-Crank J, Dukes ID, Chandy G, Hustad CM, Copeland NG, et al. Genomic organization, chromosomal localization, tissue distribution, and biophysical characterization of a novel mammalian Shaker-related voltage-gated potassium channel, Kv1.7. *J Biol Chem* 1998; 273: 5851–7.
- 33) Kerschensteiner D, Soto F, Stocker M. Fluorescence measurements reveal stoichiometry of K<sup>+</sup> channels formed by modulatory and delayed rectifier alpha-subunits. *Proc Natl Acad Sci U S A*. 2005; 102(17): 6160–5.
- 34) Kramer JW, Post MA, Brown AM, Kirsch GE. Modulation of potassium channel gating by co-expression of Kv2.1 with regulatory Kv5.1 or Kv6.1 alpha-subunits. *Am J Physiol* 1998; 274: 1501–10.
- 35) Kuo HC, Cheng CF, Clark RB, Lin JJ, Lin JL, Hoshijima M, Nguyễn-Trần VT, Gu Y, Ikeda Y, Chu PH, Ross J, Giles WR, Chien KR. A defect in the Kv channel-interacting protein 2 (KCHIP2) gene leads to a complete loss of I(to) and confers susceptibility to ventricular tachycardia. *Cell* 2001; 107(6):801-13.

- 36) Lesage F, Lazdunski M. Molecular and functional properties of two-pore-domain potassium channels. *Am J Physiol Renal Physiol.* 2000; 279(5): F793–801.
- 37) Lundby A, Olesen SP. KCNE3 is an inhibitory subunit of the Kv4.3 potassium channel. *Biochem Biophys Res Commun* 2006; 346(3):958-67.
- 38) Lundquist AL, Manderfield LJ, Vanoye CG, Rogers CS, Donahue BS, Chang PA, Drinkwater DC, Murray KT, George AL. Expression of multiple KCNE genes in human heart may enable variable modulation of I(Ks). *J Mol Cell Cardiol* 2005; 38: 277–87.
- 39) Marbán E. Heart failure: the electrophysiologic connection. *J Cardiovasc Electrophysiol.* 1999; 10(10): 1425–8.
- 40) Mazhari R, Nuss HB, Armoundas AA, Winslow RL, Marbán E. Ectopic expression of KCNE3 accelerates cardiac repolarization and abbreviates the QT interval. *J Clin Invest* 2002; 109(8):1083-90.
- 41) McCrossan ZA, Abbott GW. The MinK-related peptides. *Neuropharmacology* 2004; 47: 787–821
- 42) McDonald TV, Yu Z, Ming Z, Palma E, Meyers MB, Wang KW, Goldstein SA, Fishman GI. A minK–HERG complex regulates the cardiac potassium current I(Kr). *Nature* 1997; 388: 289–92.
- 43) Mitcheson JS, Chen J, Lin M, Culberson C, Sanguinetti MC. A structural basis for drug-induced long QT syndrome. *Proc Natl Acad Sci U S A.* 2000; 97(22): 12329–33.
- 44) Nattel S, Yue L, Wang Z. Cardiac ultrarapid delayed rectifiers: a novel potassium current family of functional similarity and molecular diversity. *Cell Physiol Biochem.* 1999; 9(4–5): 217–26.
- 45) Nerbonne JM, Kass RS. Molecular physiology of cardiac repolarization. *Physiol Rev.* 2005; 85(4): 1205–53.
- 46) Noda M, Shimizu S, Tanabe T, Takai T, Kayano T, Ikeda T, Takahashi H, Nakayama H, Kanaoka Y, Minamino N, et al. Primary structure of *Electrophorus electricus* sodium channel deduced from cDNA sequence. *Nature.* 1984; 312(5990):121–7.
- 47) Ohya S, Tanaka M, Oku T, Asai Y, Watanabe M, Giles WR, Imaizumi Y. Molecular cloning and tissue distribution of an alternatively spliced variant of an A-type K<sup>+</sup> channel alpha-subunit, Kv4.3 in the rat. *FEBS Lett* 1997; 420: 47– 53.
- 48) Ordog B, Brutyo E, Puskas LG, Papp JG, Varro A, Szabad J, Boldogkoi Z. Gene expression profiling of human cardiac potassium and sodium channels. *Int J Cardiol.* 2006; 111(3): 386–93.
- 49) Ottschytch N, Raes A, Van Hoorick D, Snyders DJ. Obligatory heterotetramerization of three previously uncharacterized Kv channel alpha-subunits identified in the human genome. *Proc Natl Acad Sci U S A* 2002; 99: 7986–91.
- 50) Paddison PJ, Cleary M, Silva JM, Chang K, Sheth N, Sachidanandam R, Hannon GJ. Cloning of short hairpin RNAs for gene knockdown in mammalian cells. *Nat Methods* 2004; 1(2):163-7.
- 51) Pak MD, Baker K, Covarrubias M, Butler A, Ratcliffe A, Salkoff L. mShal, a subfamily of A-type K<sup>+</sup> channel cloned from mammalian brain. *Proc Natl Acad Sci U S A* 1991; 88: 4386–90.
- 52) Patel AJ, Lazdunski M, Honore E. Kv2.1/Kv9.3, a novel ATP-dependent delayed-rectifier K<sup>+</sup> channel in oxygen-sensitive pulmonary artery myocytes. *EMBO J* 1997; 16: 6615–25.
- 53) Patel SP, Campbell DL. Transient outward potassium current, 'Ito', phenotypes in the mammalian left ventricle: underlying molecular, cellular and biophysical mechanisms. *J Physiol* 2005; 569(Pt 1):7-39.
- 54) Pfaffl MW, Horgan GW, Dempfle L. Relative expression software tool (REST) for group-wise comparison and statistical analysis of relative expression results in real-time PCR. *Nucleic Acids Res.* 2002; 30(9): e36.

- 55) Po S, Snyders DJ, Baker R, Tamkun MM, Bennett PB. Functional expression of an inactivating potassium channel cloned from human heart. *Circ Res* 1992; 71: 732–6
- 56) Pomeranz LE, Reynolds AE, Hengartner CJ. Molecular biology of pseudorabies virus: impact on neurovirology and veterinary medicine. *Microbiol Mol Biol Rev* 2005; 69(3):462-500.
- 57) Prorok J, Kovács PP, Kristóf AA, Nagy N, Tombácz D, Tóth JS, Ördög B, Jost N, Virág L, Papp JG, Varró A, Tóth A and Boldogkői Zs. Herpesvirus-Mediated Delivery of a Genetically Encoded Fluorescent Ca<sup>2+</sup> Sensor to Canine Cardiomyocytes. *J Biomed Biotechnol* 2009; 2009:361795.
- 58) Radicke S, Cotella D, Graf EM, Banse U, Jost N, Varró A, Tseng GN, Ravens U, Wettwer E. Functional modulation of the transient outward current I<sub>to</sub> by KCNE beta-subunits and regional distribution in human non-failing and failing hearts. *Cardiovasc Res* 2006; 71(4):695-703.
- 59) Ramsay G. DNA chips: state-of-the art. *Nat Biotechnol.* 1998; 16(1): 40–4.
- 60) Roden DM. Long QT syndrome: reduced repolarization reserve and the genetic link. *J Intern Med.* 2006; 259(1): 59–69.
- 61) Roden DM. Torsade de pointes. *Clin Cardiol.* 1993; 16(9): 683–6.
- 62) Sakmann B, Neher E. Patch clamp techniques for studying ionic channels in excitable membranes. *Annu Rev Physiol.* 1984; 46: 455–72.
- 63) Salinas M, Duprat F, Heurteaux C, Hugnot JP, Lazdunski M. New modulatory alpha subunits for mammalian Shab K<sup>+</sup> channels. *J Biol Chem* 1997; 272: 24371–9.
- 64) Sands Z, Grottesi A, Sansom MS. Voltage-gated ion channels. *Curr Biol.* 2005; 15(2): R44–7.
- 65) Sanguinetti MC, Bennett PB. Antiarrhythmic drug target choices and screening. *Circ Res.* 2003; 93(6): 491–9.
- 66) Sanguinetti MC, Curran ME, Zou A, Shen J, Spector PS, Atkinson DL, Keating MT. Coassembly of K(V)LQT1 and minK (IsK) proteins to form cardiac I(Ks) potassium channel. *Nature* 1996; 384:80–3.
- 67) Schroeder BC, Waldegger S, Fehr S, Bleich M, Warth R, Greger R, Jentsch TJ. A constitutively open potassium channel formed by KCNQ1 and KCNE3. *Nature* 2000; 403(6766):196-9.
- 68) Schröter KH, Ruppersberg JP, Wunder F, Rettig J, Stocker M, Pongs O. Cloning and functional expression of a TEA-sensitive A-type potassium channel from rat brain. *FEBS Lett* 1991; 278: 211–6.
- 69) Serodio P, Vega-Saenz de Miera E, Rudy B. Cloning of a novel component of A-type K<sup>+</sup> channels operating at subthreshold potentials with unique expression in heart and brain. *J Neurophysiol* 1996; 75: 2174–9.
- 70) Shih HT. Anatomy of the action potential in the heart. *Tex Heart Inst J.* 1994; 21(1): 30–41.
- 71) Shorofsky SR, Balke CW. Calcium currents and arrhythmias: insights from molecular biology. *Am J Med.* 2001; 110(2): 127–40.
- 72) Stegmeier F, Hu G, Rickles RJ, Hannon GJ, Elledge SJ. A lentiviral microRNA-based system for single-copy polymerase II-regulated RNA interference in mammalian cells. *Proc Natl Acad Sci U S A.* 2005; 102(37):13212-7.
- 73) Svensson EC, Marshall DJ, Woodard K, Lin H, Jiang F, Chu L, Leiden JM. Efficient and stable transduction of cardiomyocytes after intramyocardial injection or intracoronary perfusion with recombinant adeno-associated virus vectors. *Circulation* 1999; 99(2):201-5.
- 74) Szentadrassy N, Banyasz T, Biro T, Szabo G, Toth BI, Magyar J, Lazar J, Varro A, Kovacs L, Nanasi PP. Apico-basal inhomogeneity in distribution of ion channels in canine and human ventricular myocardium. *Cardiovasc Res* 2005; 65: 851–60.

- 75) Varro A, Baláti B, Iost N, Takács J, Virág L, Lathrop DA, Csaba L, Tálosi L, Papp JG. The role of the delayed rectifier component IKs in dog ventricular muscle and Purkinje fibre repolarization. *J Physiol.* 2000; 1:67-81.
- 76) Varró A, Biliczki P, Iost N, Virág L, Hála O, Kovács P, Mátyus P, Papp JG. Theoretical possibilities for the development of novel antiarrhythmic drugs. *Curr Med Chem.* 2004; 11(1): 1–11.
- 77) Wang WK, Chen MY, Chuang CY, Jeang KT, Huang LM. Molecular biology of human immunodeficiency virus type 1. *J Microbiol Immunol Infect* 2000; 33(3):131-40.
- 78) Wang Z, Feng J, Shi H, Pond A, Nerbonne JM, Nattel S. Potential molecular basis of different physiological properties of the transient outward K<sup>+</sup> current in rabbit and human atrial myocytes. *Circ Res* 1999; 84: 551–61.
- 79) Weiser M, Vega-Saenz de Miera E, Kentros C, Moreno H, Franzen L, Hillman D, Baker H, Rudy B. Differential expression of Shaw-related K<sup>+</sup> channels in the rat central nervous system. *J Neurosci* 1994; 14: 949–72.
- 80) Wiznerowicz M, Trono D. Harnessing HIV for therapy, basic research and biotechnology. *Trends Biotechnol* 2005; 23(1):42-7.
- 81) Yang N, George AL, Horn R. Molecular basis of charge movement in voltage-gated sodium channels. *Neuron* 1996; 16(1): 113–22.
- 82) Yue L, Feng J, Li GR, Nattel S. Transient outward and delayed rectifier currents in canine atrium: properties and role of isolation methods. *Am J Physiol* 1996; 270:H2157-68.
- 83) Zhuo ML, Huang Y, Liu DP, Liang CC. KATP channel: relation with cell metabolism and role in the cardiovascular system. *Int J Biochem Cell Biol.* 2005; 37(4): 751–64.

## Acknowledgements

The fundamental part of the project that kept me busy during the past few years was formulated in a scientific cooperation program between the Department of Biology and the Department of Pharmacology and Pharmacotherapy of the University of Szeged. I wish to thank the ingenious efforts of Professor András Varró, Professor János Szabad and of Professor Zsolt Boldogkői for organizing both the scientific and the administrative frames of the project. I am also thankful for their advices. I am also very grateful to Dr Stanley Nattel, Director of the Electrophysiology Research Group of the Montreal Heart Institute, for providing the inspiring environment and support for the completion of the RNAi experiments. I extend my appreciation to the co-workers and fellow Ph.D. students in the two Departments of the University of Szeged, most especially to Endre Brutyó and János Prorok, who participated tremendously in the experimental work. I am also grateful to the colleagues in Professor Nattel's lab, particularly to Ling Xiao, who so kindly sacrificed a part of her patch-clamp time.

Support for my Ph.D. work came from scientific cooperation programs organized by Professor András Varró and Professor János Szabad: (1) A szívritmuszavarokhoz társuló hirtelen halál farmakológiai prevenciója (OM-00324/2002). (2) Az RNSi technika alkalmazása a hirtelen halált okozó szívritmia molekuláris alapjainak felderítésében (ETT 1280-9/2003-1018 EKU); (3) A hirtelen szívhalál megelőzésének új útjai: molekuláris biológiai, genetikai és farmakológiai vizsgálata (BIO 19541945). (4) Graduate Student Program of the University of Szeged.